A NONLINEAR POSITIVE EXTENSION OF THE LINEAR DISCONTINUOUS SPATIAL DISCRETIZATION OF THE TRANSPORT EQUATION

A Thesis

by

PETER GREGORY MAGINOT

Submitted to the Office of Graduate Studies of
Texas A&M University
in partial fulfillment of the requirements for the degree of

MASTER OF SCIENCE

December 2010

Major Subject: Nuclear Engineering

A NONLINEAR POSITIVE EXTENSION OF THE LINEAR DISCONTINUOUS SPATIAL DISCRETIZATION OF THE TRANSPORT EQUATION

A Thesis

by

PETER GREGORY MAGINOT

Submitted to the Office of Graduate Studies of
Texas A&M University
in partial fulfillment of the requirements for the degree of

MASTER OF SCIENCE

Approved by:

Co-Chairs of Committee,	Jim Morel
	Jean Ragusa
Committee Members,	Marvin Adams
	Jean-Luc Guermond
Head of Department,	Raymond Juzaitis

December 2010

Major Subject: Nuclear Engineering

ABSTRACT

A Nonlinear Positive Extension of the Linear Discontinuous Spatial Discretization of the Transport Equation. (December 2010)

Peter Gregory Maginot, B.S. Nuclear Engineering, Texas A&M University

Co-Chairs of Advisory Committee: Dr. Jim Morel
Dr. Jean Ragusa

Linear discontinuous (LD) spatial discretization of the transport operator can generate negative angular flux solutions. In slab geometry, negativities are limited to optically thick cells. However, in multi-dimension problems, negativities can even occur in voids. Past attempts to eliminate the negativities associated with LD have focused on inherently positive solution shapes and ad-hoc fixups. We present a new, strictly non-negative finite element method that reduces to the LD method whenever the LD solution is everywhere positive. The new method assumes an angular flux distribution, $\widetilde{\psi}$, that is a linear function in space, but with all negativities set-to-zero. Our new scheme always conserves the zeroth and linear spatial moments of the transport equation. For these reasons, we call our method the consistent set-to-zero (CSZ) scheme.

CSZ can be thought of as a nonlinear modification of the LD scheme. When the LD solution is everywhere positive within a cell, $\widetilde{\psi}_{csz} = \widetilde{\psi}_{LD}$. If $\widetilde{\psi}_{LD} < 0$ somewhere within a cell, $\widetilde{\psi}_{csz}$ is a linear function $\hat{\psi}_{csz}$ with all negativities set to zero. Applying CSZ to the transport moment equations creates a nonlinear system of equations which is solved to obtain a non-negative solution that preserves the moments of the transport equation. These properties make CSZ unique; it encompasses the desirable properties of both strictly positive nonlinear solution representations and ad-hoc fixups. Our test problems indicate that CSZ avoids the slow spatial convergence properties of past inherently positive solutions representations, is more accurate than

ad-hoc fixups, and does not require significantly more computational work to solve a problem than using an ad-hoc fixup.

Overall, CSZ is easy to implement and a valuable addition to existing transport codes, particularly for shielding applications. CSZ is presented here in slab and rectangular geometries, but is readily extensible to three-dimensional Cartesian (brick) geometries. To be applicable to other simulations, particularly radiative transfer, additional research will need to be conducted, focusing on the diffusion limit in multi-dimension geometries and solution acceleration techniques.

ACKNOWLEDGMENTS

An extra thanks is extended to Dr. Morel and Dr. Ragusa for their years of guidance and continued assistance in this and other ventures.

Partial funding of this research came from the Department of Energy Computational Science Graduate Fellowship under grant DE-FG02-97ER25308.

NOMENCLATURE

CSZ	Consistent Set-to-Zero
ED	Exponential Discontinuous
LC	Linear Characteristic
LD	Linear Discontinuous
S_N	Discrete Ordinates Method
WL	Warsa-Like

TABLE OF CONTENTS

Page

Page

LIST OF TABLES

LIST OF FIGURES

FIGURE Page

1. INTRODUCTION

A variety of spatial discretizations used in the S_N treatment of the Boltzmann radiation transport equation can result in non-physical, negative angular flux solutions [1]. Small negativities do not necessarily affect the overall accuracy of a method [2], but the effect of negative negative angular flux solutions is highly problem dependent. One popular method of S_N spatial discretization is the finite element, linear discontinuous (LD) differencing scheme. LD is popular for many reasons: it is straight forward, yields 3rd order convergence for the cell average and outflow angular fluxes in 1D, and is pointwise 2nd order convergent for multidimension calculations [3]. In 1D Cartesian geometry, LD produces negativities only in optically thick cells, and the negativities are quickly damped. However, in multidimensional Cartesian geometries, LD can generate significant negative angular flux solutions in void regions. Negativities are not limited to discontinuous differencing schemes. Higher-order characteristic methods such as the linear characteristic (LC) method can also produce negative angular flux solutions when the scattering source expansion becomes negative [4]. Likewise, the diamond difference scheme is notorious for yielding large, essentially undamped negativities, under a variety of conditions [1].

1.1 Past Work

Past work to eliminate the calculation of negative angular flux solutions has focused on two areas:

1. ad-hoc fixups and

2. strictly non-negative, nonlinear angular flux representations.

This thesis follows the style of the Journal of Computational Physics.

An example of an ad-hoc fixup scheme would be the diamond-difference scheme with set-to-zero flux fixup [1]. The use of ad-hoc fixups always works for pure absorbers. Traditionally ad-hoc fixups have interacted poorly with advanced convergence acceleration schemes, such as diffusion synthetic acceleration (DSA) [5], in highly scattering problems, where such advanced convergence techniques are most needed. As such, ad-hoc fixup methods are often not acceptable for a large class of problems. However, very recent research [6] has indicated that the difficulties associated with ad-hoc fixups and advanced acceleration techniques has largely been caused by the use of fixed point iteration techniques rather than Newton's method to solve the associated equations.

Several inherently non-negative solution representations have been investigated in the past, more so for characteristic schemes than discontinuous differencing schemes. Characteristic schemes yield strictly positive angular flux solutions given strictly non-negative scattering sources; so, one needs to represent the scattering source in a strictly positive way, rather than the solution itself. Strictly non-negative, nonlinear characteristic schemes examined in the past have included: the exponential, step adaptive, and linear adaptive characteristic schemes. The exponential characteristic schemes developed independently by Mathews, et. al [7] [8] and Walters and Wareing [9] assume an exponential source distribution with an exponent that is linear in space. Mathews has also developed the step adaptive and linear adaptive characteristic methods [10] [11]. The step adaptive method assumes that within a cell, the scattering source is a constant positive value over some portion of the cell and 0 everywhere else; whereas the linear adaptive scheme assumes the scattering source is represented by a linear function over the cell, but with all negativities set to zero.

For discontinuous differencing, two strictly non-negative solution representation have been tried to date, the step discontinuous differencing scheme [1] and the exponential discontinuous (ED) scheme developed by Wareing [12]. Though both produce strictly non-negative solutions, neither method is ideal. The step scheme is only first

order accurate, which is obviously undesirable as an alternative to LD which can be up to 3rd order accurate. ED asymptotically converges at the same rate as LD. However, the relative accuracy of LD and ED is problem dependent. For some problems, ED is more accurate than LD; for other problems, LD is more accurate [12].

1.2 New Method

Our purpose here is to devise a new nonlinear spatial finite-element method for 1-D and 2-D Cartesian geometries. This method has two central characteristics: first, the new scheme is equivalent to LD whenever LD yields a strictly positive solution, and second, the scheme always satisfies both the zero'th and first spatial moment equations, which standard ad-hoc fixups do not satisfy.

Work for this thesis began as a multi-dimensional extension of the strictly positive finite-element closure presented at Saratoga [13]. However, we encountered difficulties that, together with the results of Fichtl and Warsa [6], motivated us to develop a fundamentally different approach. The new method presented herein represents the discontinuous finite-element analog of the linear adaptive characteristic scheme originally developed for both slab and rectangular geometries by Mathews et al. [10,11]. Qualitatively, the new method assumes an angular flux distribution within a cell that is defined to be equal to a linear function at all points for which that function is positive and zero at all points for which the linear function is negative. Since the zero'th and first spatial moments of the transport equation are rigorously solved with our method, and the distribution is obtained from a linear function via a set-to-zero procedure, we refer to our new finite element method as the consistent set-to-zero method (CSZ).

The remainder of this thesis is divided into 6 sections, derivations in slab geometry, derivations in rectangular geometry, solution techniques, computational results for slab test problems, computational results in rectangular geometry, and finally conclusions.

2. SLAB GEOMETRY EQUATION DERIVATION

2.1 Slab Geometry Moment Equations

The S_N transport equation in 1D Cartesian geometry is

$$\mu_d \frac{d\psi}{dx} + \sigma_t \psi(\mu_d, x) = S(\mu_d, x)\,, \tag{2.1}$$

with discrete direction d, $\psi(\mu_d, x)$ as the angular flux with direction cosine μ_d, at position x, total interaction cross section σ_t, and a total fixed and scattering source S that is also a function of x and μ_d. We begin our derivation by taking the zero-th and first spatial moments of Eq. (2.1) in cell i. Cell i is centered on x_i with edges $x_{i-1/2}$ and $x_{i+1/2}$ and characteristic width $\Delta x_i = x_{i+1/2} - x_{i-1/2}$. For simplicity, we first make the transformation to a reference element, $x \in [x_{i-1/2}, x_{i+1/2}] \rightarrow s \in [0, 1]$:

$$x = x_{i-1/2} + s\Delta x_i\,, \tag{2.2}$$

where one can easily verify that $x = x_{i-1/2}$ when $s = 0$ and $x = x_{i+1/2}$ when $s = 1$. With this transformation, we take the zero-th and first spatial moments of Eq. (2.1) by multiplying with basis functions

$$P_0(s) = 1\,, \tag{2.3}$$

$$P_1(s) = 2s - 1\,, \tag{2.4}$$

and integrating over cell i. The resultant moment equations are:

$$\frac{\mu_d}{\Delta x_i}\left(\psi_{i+1/2,d} - \psi_{i-1/2,d}\right) + \sigma_{t,i}\psi_{A,i,d} = S_{A,i,d}\,, \tag{2.5a}$$

$$\frac{3\mu_d}{\Delta x_i}\left(\psi_{i+1/2,d} - \psi_{i-1/2,d} - 2\psi_{A,i,d}\right) + \sigma_{t,i}\psi_{X,i,d} = S_{X,i,d}\,, \tag{2.5b}$$

where the d subscript denotes quantities specific to angular flux with direction cosine μ_d. $\psi_{i-1/2,d}$ and $\psi_{i+1/2,d}$ are defined as:

$$\psi_{i-1/2,d} = \psi(\mu_d, 0)\,, \tag{2.6}$$

$$\psi_{i+1/2,d} = \psi(\mu_d, 1)\,. \tag{2.7}$$

The average and slope quantities, $\psi_{A,i,d}$ and $\psi_{X,i,d}$, are defined as:

$$\psi_{A,i,d} = \int_0^1 P_0(s)\psi(\mu_d, s)ds\,, \tag{2.8a}$$

$$\psi_{X,i,d} = 3\int_0^1 P_1(s)\psi(\mu_d, s)ds\,. \tag{2.8b}$$

Equation 2.5 has three unknowns, $\psi_{A,i,d}$, $\psi_{X,i,d}$, and the cell outflow, $\psi_{i\pm1/2,d}$, depending on the sign of μ_d. For brevity, we limit our treatment to $\mu_d > 0$ so that $\psi_{i+1/2,d}$ is the cell outflow and $\psi_{i-1/2,d}$ is the known inflow angular flux. To solve the moment equations and close the system of two equations with three unknowns, a distribution for the angular flux, $\widetilde{\psi}(s)$, within the cell must be assumed.

2.2 LD Derivation

The LD scheme assumes a linear angular flux distribution within each cell:

$$\widetilde{\psi}(s)_{LD} = a_{LD}P_0(s) + b_{LD}P_1(s)\,. \tag{2.9}$$

Applying the definitions of Eq. (2.6) and Eq. (2.8), the LD relationships for the cell unknowns become:

$$\psi_{A,i,d} = a_{LD}\,, \tag{2.10a}$$

$$\psi_{X,i,d} = b_{LD}\,, \tag{2.10b}$$

$$\psi_{i+1/2,d} = a_{LD} + b_{LD}\,. \tag{2.10c}$$

Inserting the definitions of Eq. (2.10) into the moment equations of Eq. (2.5) creates a system of two linear equations entirely defined in terms of a_{LD}, and b_{LD}, which then completely defines $\widetilde{\psi}(s)_{LD}$ within cell i. Because the relationships in Eqs. (2.10) are linear, one can directly solve for a_{LD} and b_{LD} in terms of $\psi_{A,i,d}$ and $\psi_{X,i,d}$ making $\psi_{A,i,d}$ and $\psi_{X,i,d}$ the primary unknowns.

2.3 ED Derivation

To compare the CSZ scheme to previously developed strictly positive nonlinear solution representations, we now derive the ED scheme. The ED method assumes an exponential representation for the angular flux within a cell. By assuming an exponential representation, Eq. (2.5) becomes a nonlinear system of equations. For the ED scheme, the exact formulation of the $\widetilde{\psi}(s)$ can take on several different forms; however all forms must be equivalent to a linear exponential. We define a linear exponential to be the exponential function with an exponent that is linear in space. In Wareing's development of the exponential discontinuous finite-element method [12], the flux distribution $\widetilde{\psi}$ was represented as:

$$\widetilde{\psi}(x) = c_1 e^{c_2 P_{1S}(s)} \,. \tag{2.11}$$

In our replication of ED (for comparison purposes), we formulate $\widetilde{\psi}$ slightly differently. To ensure that the exponential remains positive at all times, the magnitude controlling parameter, c_1, was moved into the exponential term:

$$\widetilde{\psi}(s)_{ED} = e^{c_1 P_0(s) + c_2 P_1(s))} \,. \tag{2.12}$$

Hereafter, ED will be synonymous with the formulation described by Eq. (2.12). The reader is directed to [12] for a more complete derivation based on Eq. (2.11), including applications in multidimension Cartesian geometries. The definitions of $\psi_{A,i,d}$, $\psi_{X,i,d}$, and $\psi_{i+1/2,d}$ for ED are given below:

$$\psi_{A,i,d} = \frac{e^{c_1}}{2c_2}\left(e^{c_2} - e^{-c_2}\right) \,, \tag{2.13a}$$

$$\psi_{X,i,d} = \frac{3}{2{c_2}^2}\left((c_2 - 1)e^{c_1+c_2} + (c_2 + 1)e^{c_1-c_2}\right) \,, \tag{2.13b}$$

$$\psi_{i+1/2,d} = e^{c_1+c_2} \,. \tag{2.13c}$$

Unlike LD, the relationships in Eqs. (2.13), are nonlinear and cannot be directly inverted to express c_1 and c_2 in terms of $\psi_{A,i,d}$ and $\psi_{X,i,d}$. Thus c_1 and c_2 must remain the primary unknowns. As with LD, inserting the definitions of Eq. (2.13)

into Eq. (2.5) creates a system of two equations defined entirely in terms of only two unknowns, c_1 and c_2, which then fully define $\widetilde{\psi}_{ED}(s)$. However, unlike the LD system of equations, this system of equations is nonlinear. Discussions pertaining to the solution techniques employed are provided in Section 4.

2.4 CSZ Derivation

Let us now define our CSZ scheme, which is a strictly non-negative modification of the LD scheme. One of the primary objectives of the CSZ scheme is to yield the LD solution whenever that solution is everywhere positive within the cell. As such, CSZ first determines $\widetilde{\psi}_{LD}$. If $\widetilde{\psi}_{LD}$ is positive everywhere in the interval $s \in [0, 1]$, $\widetilde{\psi}_{csz} = \widetilde{\psi}_{LD}$ and no further work is required. However, if $\widetilde{\psi}_{LD}$ is not everywhere positive, $\widetilde{\psi}_{csz}$ is represented by a linear function, $\hat{\psi}_{csz}$,

$$\hat{\psi}_{csz}(s) = a_{csz} P_0(s) + b_{csz} P_1(s)\,, \tag{2.14}$$

with all negativities set to zero.

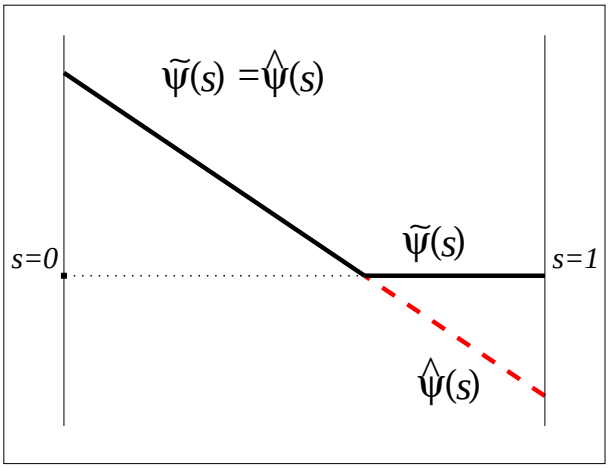

Fig. 2.1. Graphical definition of $\widetilde{\psi}_{csz}(s)$ on $[0, 1]$.

The behavior of $\widetilde{\psi}_{csz}(s)$ is graphically displayed in Fig. 2.1, which is identical to the following definition:

$$\widetilde{\psi}_{csz}(s) = \begin{cases} \hat{\psi}_{csz}(s) & \text{if} \quad \hat{\psi}_{csz}(s) \geq 0 \\ 0 & \text{otherwise} \end{cases} . \tag{2.15}$$

It must be emphasized that the parameters, a_{csz} and b_{csz}, describing $\hat{\psi}_{csz}$ are *not* equal to their LD counterparts, a_{LD} and b_{LD}, if $\hat{\psi}_{csz}(s) < 0$ for any $s \in [0, 1]$.

For slab geometries, $\widetilde{\psi}_{csz}(s)$ in cell i can be one of three following cases:

1. positive everywhere (LD definitions apply – Eq. (2.10)) or,
2. positive $s < s_z$ or,
3. positive $s > s_z$.

The following definitions relate only to the CSZ method when $\hat{\psi}_{csz}(s)$ is not strictly positive within a cell. First, we denote s_z as the abscissa position within a cell such that $\hat{\psi}_{csz}(s_z) = 0$. s_z is simply given by:

$$s_z = \frac{1}{2}\left(1 - \frac{a_{csz}}{b_{csz}}\right) . \tag{2.16}$$

Since $\widetilde{\psi}_{csz}(s)$ is 0 over a portion of a cell, in cases 2 and 3, the spatial integrations in Eq. (2.8a) and Eq. (2.8b) can be restricted to the portion of the cell where $\widetilde{\psi}_{csz} \geq 0$. For case 2, integrating over the interval $[0, s_z]$ yields:

$$\psi_{A,i,d} = s_z \left(a_{csz} + (s_z - 1)b_{csz}\right) , \tag{2.17a}$$

$$\psi_{X,i,d} = s_z \left(4b_{csz}{s_z}^2 + 3\left(b_{csz}(1 - 2s_z) + a_{csz}(s_z - 1)\right)\right) . \tag{2.17b}$$

In slab geometry the cell outflow, $\psi_{i+1/2,d}$ is simply the value of $\widetilde{\psi}(1)$. Applying Eq. (2.15), we have:

$$\psi_{i+1/2,d} = \begin{cases} a_{csz} + b_{csz} & \text{if} \quad \hat{\psi}_{csz}(1) \geq 0 \\ 0 & \text{otherwise} \end{cases} . \tag{2.18}$$

Equations for case 3 can be found in Appendix A. Since s_z is a function only of the variables a_{csz} and b_{csz}, Eq. (2.17a), Eq. (2.17b), and Eq. (2.18), are all functions of a_{csz} and b_{csz}. Thus, inserting the definitions of Eq. (2.17a), Eq. (2.17b), and Eq. (2.18) into the moment equations, Eq. (2.5), creates a system of two nonlinear equations dependent on only two unknowns, a_{csz} and b_{csz}.

3. RECTANGULAR GEOMETRY EQUATION DERIVATION

3.1 Rectangular Geometry Moment Equations

In rectangular geometry, the transport equation becomes:

$$\mu_d \frac{\partial \psi}{\partial x} + \eta_d \frac{\partial \psi}{\partial y} + \sigma_t \psi = S \,, \tag{3.1}$$

where both ψ and S are functions of the variables position variables$x,\ y$ and direction variables η_d, and μ_d, and σ_t is the total interaction cross section. We begin our derivation by first taking the spatial moments of Eq. (3.1) within cell i, j. Cell $i,\ j$ is centered at (x_i, y_j), with characteristic widths Δx_i and Δy_j, and edges and vertices numbered as in Fig. 3.1: Again, we begin taking the moments by first transforming

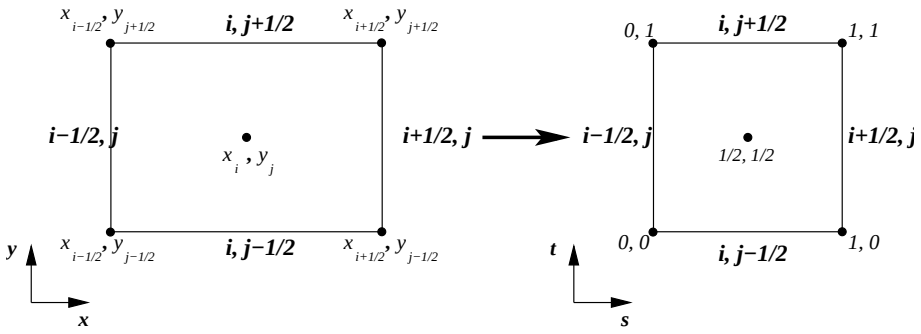

Fig. 3.1. Graphical explanation of the nomenclature associated with cell $i,\ j$.

into a general reference frame:

$$x = x_{i-1/2} + \Delta x_i s \,, \tag{3.2}$$

$$y = y_{j-1/2} + \Delta y_j t \,. \tag{3.3}$$

The moments within cell $i,\ j$ are taken by first multiplying by basis functions:

$$P_0(s,t) = 1 \,, \tag{3.4}$$

$$P_{1S}(s,t) = 2s - 1 \,, \tag{3.5}$$

$$P_{1T}(s,t) = 2t - 1 \,, \tag{3.6}$$

then integrating over the transformed cell $i,\ j$. With this we obtain the following moment equations of Eq. (3.1):

$$\frac{\mu_d}{\Delta x_i}\left(\psi_{i+1/2,j,d}-\psi_{i-1/2,j,d}\right)+\frac{\eta_d}{\Delta y_j}\left(\psi_{i,j+1/2,d}-\psi_{i,j-1/2,d}\right) + \sigma_{t,i,j}\psi_{A,i,j,d}=S_{A,i,j,d}\,, \quad (3.7a)$$

$$\frac{3\mu_d}{\Delta x_i}\left(\psi_{i+1/2,j,d}+\psi_{i-1/2,j,d}-2\psi_{A,i,j,d}\right)+\frac{\eta_d}{\Delta y_j}\left(\psi_{M,i,j+1/2,d}-\psi_{M,i,j-1/2,d}\right) + \sigma_{t,i,j}\psi_{X,i,j,d}=S_{X,i,j,d}\,, \quad (3.7b)$$

$$\frac{\mu_d}{\Delta x_i}\left(\psi_{M,i+1/2,j,d}-\psi_{M,i-1/2,j,d}\right)+\frac{3\eta_d}{\Delta y_j}\left(\psi_{i,j+1/2,d}+\psi_{i,j-1/2,d}-2\psi_{A,i,j,d}\right) + \sigma_{t,i,j}\psi_{Y,i,j,d}=S_{Y,i,j,d}\,. \quad (3.7c)$$

Equations 3.7 apply to all directions, but for conciseness and without loss of generality, we limit our treatment to $\mu_d > 0$, $\eta_d > 0$. For $\mu_d > 0$ and $\eta_d > 0$, the known inflow quantities are $\psi_{i,j-1/2,d}$, $\psi_{i-1/2,j,d}$, $\psi_{X,i,j-1/2,d}$, and $\psi_{Y,i-1/2,j,d}$, and the unknown outflow quantities are $\psi_{i,j+1/2,d}$, $\psi_{i+1/2,j,d}$, $\psi_{X,i,j+1/2,d}$, and $\psi_{Y,i+1/2,j,d}$. The edge unknowns are defined as:

$$\psi_{i+1/2,j,d} = \int_0^1 \psi(1,t)dt\,, \quad (3.8a)$$

$$\psi_{i,j+1/2,d} = \int_0^1 \psi(s,1)ds\,, \quad (3.8b)$$

$$\psi_{M,i+1/2,j,d} = 3\int_0^1 P_{1T}(1,t)\psi(1,t)dt\,, \quad (3.8c)$$

$$\psi_{M,i,j+1/2,d} = 3\int_0^1 P_{1S}(s,1)\psi(s,1)ds\,. \quad (3.8d)$$

The unknown cell integral quantities of Eqs. (3.7), $\psi_{A,i,j,d}$, $\psi_{X,i,j,d}$, and $\psi_{Y,i,j,d}$, regardless of streaming direction, are defined as follows:

$$\psi_{A,i,j,d} = \int_0^1 \int_0^1 P_0(s,t)\psi(s,t)dsdt\,, \tag{3.9a}$$

$$\psi_{X,i,j,d} = 3\int_0^1 \int_0^1 P_{1S}(s,t)\psi(s,t)dsdt\,, \tag{3.9b}$$

$$\psi_{Y,i,j,d} = 3\int_0^1 \int_0^1 P_{1T}(s,t)\psi(s,t)dsdt\,. \tag{3.9c}$$

As in slab geometry, the moment equations, Eq. (3.7), have more unknowns than equations and thus require the assumption of an angular flux representation, $\widetilde{\psi}(s,t)$, in order to close the system of equations.

3.2 LD Derivation

In 2D Cartesian geometry, the LD scheme assumes an angular flux distribution that is linear in s and t:

$$\widetilde{\psi}_{LD}(s,t) = a_{LD}P_0(s,t) + b_{LD}P_{1S}(s,t) + c_{LD}P_{1T}(s,t)\,. \tag{3.10}$$

Applying the definitions of Eq. (3.8) and Eq. (3.9) yields the following relations for the unknowns of Eq. (3.7), entirely in terms of 3 unknowns, a_{LD}, b_{LD}, and c_{LD}:

$$\psi_{i,j+1/2,d} = a_{LD} + c_{LD}\,, \tag{3.11a}$$

$$\psi_{i+1/2,j,d} = a_{LD} + b_{LD}\,, \tag{3.11b}$$

$$\psi_{M,i+1/2,j,d} = c_{LD}\,, \tag{3.11c}$$

$$\psi_{M,i,j+1/2,d} = b_{LD}\,, \tag{3.11d}$$

and

$$\psi_{A,i,j,d} = a_{LD}\,, \tag{3.12a}$$

$$\psi_{X,i,j,d} = b_{LD}\,, \tag{3.12b}$$

$$\psi_{Y,i,j,d} = c_{LD}\,. \tag{3.12c}$$

$\widetilde{\psi}_{LD}(s,t)$ is then found by inserting Eq. (3.11) and Eq. (3.12) into the moment equations, Eq. (3.7). This substitution then forms a 3×3 linear system of equations defined entirely in terms of a_{LD}, b_{LD}, and c_{LD}, which in turn defines $\widetilde{\psi}_{LD}(s,t)$.

3.3 CSZ Edge Derivation

We now extend our new scheme to 2D Cartesian geometries. The basic principle of the closure remains the same as in 1D: $\widetilde{\psi}_{csz}(s,t)$ is a linear function, $\hat{\psi}_{csz}(s,t)$,

$$\hat{\psi}_{csz}(s,t) = a_{csz} + b_{csz} P_{1S}(s,t) + c_{csz} P_{1T}(s,t)\,, \tag{3.13}$$

with the negativities of $\hat{\psi}_{csz}(s,t)$ set to zero:

$$\widetilde{\psi}_{csz}(s,t) = \begin{cases} \hat{\psi}_{csz}(s,t) & \text{if } \hat{\psi}_{csz}(s,t) \geq 0 \\ 0 & \text{otherwise} \end{cases}\,. \tag{3.14}$$

Again, one of the primary objectives of the CSZ scheme is to yield the LD solution whenever LD is everywhere positive within cell $i,\ j$. As such the CSZ scheme starts by first finding the LD solution within the cell and uses $\widetilde{\psi}_{LD}(s,t)$ as the initial trial of $\hat{\psi}_{csz}(s,t)$. If $\widetilde{\psi}_{LD}(s,t) \geq 0$ everywhere within the cell, then no further work is required, $\widetilde{\psi}_{LD} = \hat{\psi}_{csz}(s,t) = \widetilde{\psi}_{csz}$.

If $\hat{\psi}_{csz} < 0$ somewhere within cell i,j (i.e., the LD solution is negative somewhere within cell $i,\ j$), then the CSZ scheme has new definitions for the unknowns defined by Eq. (3.8) and Eq. (3.9). We begin by looking at the edge unknowns defined by Eq. (3.8). Focusing our attention now on edge $i, j+1/2$, but without loss of generality, we note that along the edge $\widetilde{\psi}_{csz}$ can be:

1. everywhere positive (LD outflow definitions of Eq. (3.11)), or
2. positive $s < s_z$, or
3. positive $s > s_z$, or
4. everywhere 0

where s_z is the point where $\hat{\psi}_{csz} = 0$ along edge $i, j + 1/2$:

$$s_z = \frac{1}{2}\left(1 - \frac{a_{csz} + c_{csz}}{b_{csz}}\right) . \tag{3.15}$$

The integration of case 1 is obvious (see section 3.2). The integration of case 4 is also trivial, therefore we limit ourselves to describing case 2 here leaving a derivation of case 3 for side $i, j + 1/2$ and the complete derivation of the equations for side $i + 1/2, j$ for Appendix A. The integrals defined in Eq. (3.8b) and Eq. (3.8d) can be limited to the non-trivial portion of edge $i, j + 1/2$. For case 2, we need only to integrate over $[0, s_z]$, yielding the following results:

$$\psi_{i,j+1/2,d} = s_z \left(a_{csz} + c_{csz} + b_{csz}(s_z - 1)\right) , \tag{3.16}$$

$$\psi_{M,i,j+1/2,d} = s_z \left(3(b_{csz} - a_{csz} - c_{csz}) + 3s_z(a_{csz} - 2b_{csz} + 3c_{csz}) + 4b_{csz}s_z^2\right) . \tag{3.17}$$

3.4 CSZ Cell Derivation

Next, we seek to calculate the interior quantities, $\psi_{A,i,j,d}$, $\psi_{X,i,j,d}$, and $\psi_{Y,i,j,d}$. First, we consider the shape of the non zero portion of $\widetilde{\psi}_{csz}(s, t)$ within cell i, j. On the interior of cell i, j, $\widetilde{\psi}_{csz}$ can be:

1. everywhere positive (LD definitions apply; see Eq. (3.12)) or,
2. $\widetilde{\psi}_{csz} > 0$ at 3 of 4 corners or,
3. $\widetilde{\psi}_{csz} > 0$ at 2 of 4 corners or,
4. $\widetilde{\psi}_{csz} > 0$ at 1 of 4 corners or,
5. everywhere 0.

Fig. 3.2 illustrates the above cases. The integration is trivial for cases 1 and 5. However, integration for cases 2-4 is not a simple task as it requires the use of variable limits of integration. We have chosen to decompose the cell into triangles,

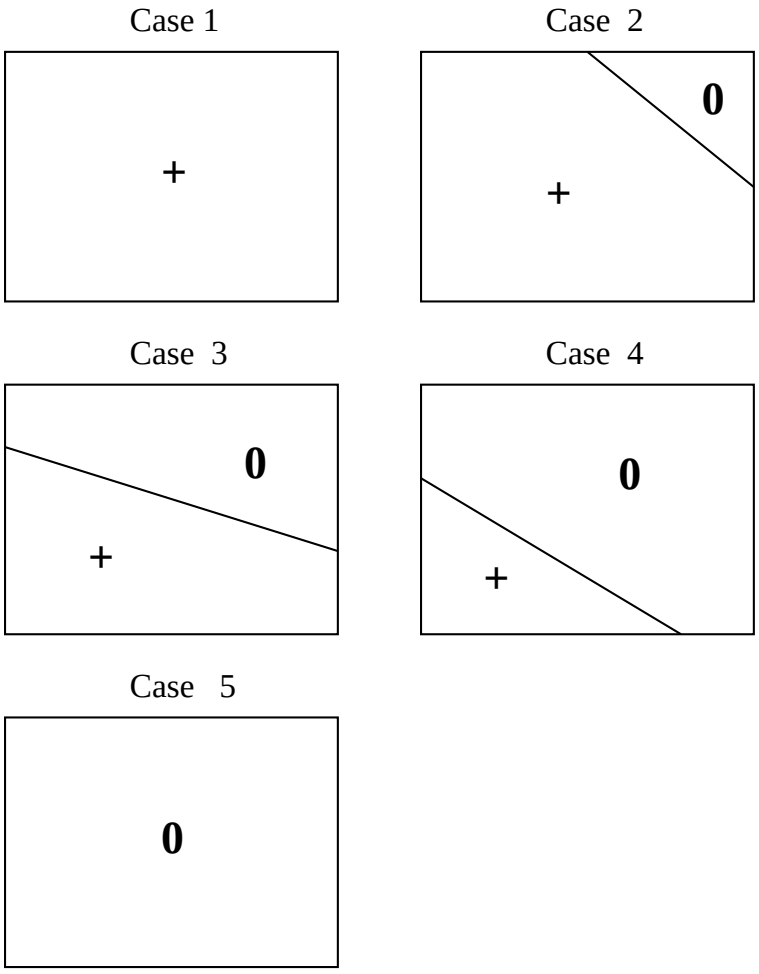

Fig. 3.2. All possible forms of the interior cell shape $\widetilde{\psi}(s,t)$ in the CSZ method.

change variables into barycentric coordinates, and then integrate the functions of interest using barycentric coordinates. Cases 2-4 are decomposed into triangular areas as shown in Fig. 3.3. The vertex points of every triangle are either vertex

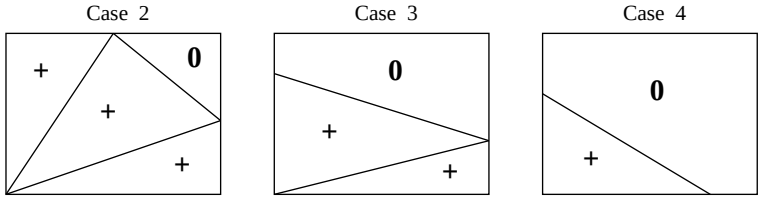

Fig. 3.3. Triangular decomposition of $\widetilde{\psi}_{CSZ}(s,t)$ in cell $i,\ j$.

points of cell i, j or a point where $\hat{\psi}_{csz}(s,t) = 0$. Each triangle T with area A has vertices $\mathbf{v_i} = (s_i, t_i)$ as shown in Fig. 3.4.

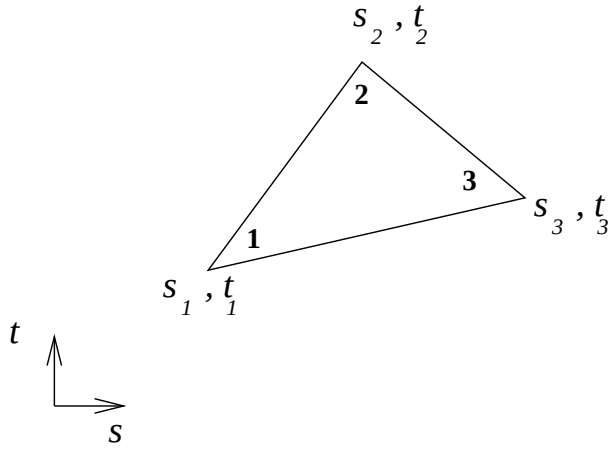

Fig. 3.4. Illustration of the coordinates of triangle T.

Barycentric integration of a function f over T takes the following form [14]:

$$\int_{\mathbf{T}} f(\mathbf{r})dr = 2A \int_0^1 \int_0^{1-\lambda_2} f\left(\lambda_1 \mathbf{v_1} + \lambda_2 \mathbf{v_2} + (1 - \lambda_1 - \lambda_2 \mathbf{v_3})\right) d\lambda_1 d\lambda_2 \,. \qquad (3.18)$$

The functions of Eq. (3.9), which are defined in terms of s and t, are converted to barycentric coordinates using the following definitions:

$$s = \lambda_1 s_1 + \lambda_2 s_2 + (1 - \lambda_1 - \lambda_2)\, s_3\,, \tag{3.19a}$$

$$t = \lambda_1 t_1 + \lambda_2 t_2 + (1 - \lambda_1 - \lambda_2)\, t_3\,. \tag{3.19b}$$

The resultant integrals were performed using the symbolic algebra program MATLAB® [15]. These integrals are omitted from this section for brevity, but may be found in Appendix A.

Similar to slab geometry, all unknowns of the rectangular geometry moment equations can be expressed completely in terms of three unknowns, a_{csz}, b_{csz}, and c_{csz}. Inserting the CSZ definitions of the rectangular cell unknowns into Eq. (3.7) creates a 3×3 nonlinear system of equations defined entirely by three unknowns.

3.5 Strictly Non-Negative Ad-hoc Fixup Comparator

In slab geometry, we derived the ED scheme to serve as comparator for CSZ. The ED scheme is an example of a previously derived strictly non-negative solution representation. We derive an ad-hoc fixup to serve as a comparator to CSZ in rectangular geometry. Specifically, we compare CSZ to a rectangular geometry ad-hoc fixup we developed inspired by a scheme presented by Warsa et. al [16] for triangular meshes. Our Warsa-like (WL) scheme is a linear and strictly positive scheme for rectangular geometry only that is based on modifying the LD scheme. WL is meant to yield the LD solution when the LD solution yields strictly non-negative outflows. The properties of the WL scheme are as follows:

1. WL guarantees only positive angular flux *outflows*,
2. WL does not conserve the full set of moment equations if LD yields a negative outflow,
3. WL *does* conserve particle balance.

The WL scheme assumes a linear angular flux representation within a cell:

$$\widetilde{\psi}_{WL} = a_{WL}P_0(s,t) + b_{WL}P_{1S}(s,t) + c_{WL}P_{1T}(s,t)\,. \tag{3.20}$$

Since WL and LD are identical linear representations of $\widetilde{\psi}(x,y)$, but with different coefficients, we first introduce $\psi_{k,m}$, the value of $\widetilde{\psi}(x,y)$, at an outflow vertex k for method m, where $m = LD$ or WL. For $\mu > 0$ and $\eta > 0$, $\psi_{k,m}$ are defined as follows:

$$\psi_{1,m} = a_m - b_m + c_m\,, \tag{3.21a}$$

$$\psi_{2,m} = a_m + b_m + c_m\,, \tag{3.21b}$$

$$\psi_{3,m} = a_m + b_m - c_m\,. \tag{3.21c}$$

The equations used to find $a_{WL},\ b_{WL},$ and c_{WL} depend on the number of negative $\psi_{k,LD}$:

1. all $\psi_{k,LD} > 0$ or,
2. one $\psi_{k,LD} < 0$ or,
3. two $\psi_{k,LD} < 0$ or,
4. three $\psi_{k,LD} < 0$.

If all $\psi_{k,LD} > 0$, then we $\widetilde{\psi}_{WL} = \widetilde{\psi}_{LD}$ and no further work is required. However, if any $\psi_{k,LD} < 0$ (cases 2–4), Eq. (3.7) do not yield a linear representation of $\widetilde{\psi}(x,y)$ that is everywhere positive along the cell outflows. Thus, $\widetilde{\psi}_{LD} \neq \widetilde{\psi}_{WL}$, and a new system of equations is required to find suitable coefficients $a_{WL},\ b_{WL},$ and c_{WL} that will yield a strictly non-negative $\widetilde{\psi}_{WL}$. Without loss of generality, we consider case 2 with $\psi_{1,LD} < 0$. Based on [16], the new system of equations consists of:

1. the balance equation Eq. (3.7a),
2. an explicit statement that $\psi_{1,WL} = 0$,

3. a scaling of positive outflows, $\frac{\psi_{2,LD}}{\psi_{3,LD}} = \frac{\psi_{2,WL}}{\psi_{3,WL}}$.

For case 3, let us assume that $\psi_{1,LD}$ and $\psi_{2,LD}$ are negative. Again, drawing from Warsa's previous work for triangular meshes, the WL equations consist of

1. the balance equation,

2. an explicit statement that $\psi_{1,WL} = 0$,

3. an explicit statement that $\psi_{2,WL} = 0$.

There is no direct parallel between the rectangular mesh case 4 and the triangular mesh scheme presented in [16] since there are two outflow vertices at most in a triangular mesh, as opposed to at most three in a rectangular mesh. Since there are only three unknowns, a_{WL}, b_{WL}, and c_{WL}, to use the balance equation and three explicit statements that $\psi_{k,WL} = 0$ produces an overdetermined system and another strategy is required. For simplicity, we have assumed the following for case 4:

$$a_{WL} = 0\,, \tag{3.22a}$$

$$b_{WL} = 0\,, \tag{3.22b}$$

$$c_{WL} = 0\,. \tag{3.22c}$$

However, in our testing, we have not encountered any problem which resulted in an LD solution falling into case 4.

The use of equations other than Eqs. (3.7) to solve for the unknowns that describe $\widetilde{\psi}_{WL}$ is what makes the WL an ad-hoc fixup. The LD, ED, and CSZ always satisfy the moment equations. The WL solution only satisfies the moment equations some of the time, other instances require the introduction of auxiliary equations required to give positivity and particle conservation.

4. SOLUTION TECHNIQUES

4.1 Linear Source Iteration

The linear Boltzmann equation describing the transport of particles can be written as:

$$\mathbf{L}\Psi = \mathbf{S}\Psi + \mathbf{q}\,, \tag{4.1}$$

with $\mathbf{L}$ being the streaming plus interaction operator, $\mathbf{S}$ the scattering operator, $\mathbf{q}$ the external source term and $\mathbf{\Psi}$ the angular flux. In slab geometry,

$$\mathbf{L}\Psi = \mu\frac{\partial\psi}{\partial x} + \sigma_t\psi\,, \tag{4.2}$$

$$\mathbf{S}\Psi = \sum_{l=0}^{L}\frac{2l+1}{W}\sigma_{s,l}\phi_l P_l(\mu_d) \tag{4.3}$$

where L is the order of the scattering source expansion, W is the sum of all the weights of the angular quadrature, ϕ_l is the l-th angular moment of the angular flux:

$$\phi_l = \sum_{d=1}^{N} w_d\psi_d P_l(\mu_d\,, \tag{4.4}$$

$\sigma_{s,l}$ is the l-th order scattering cross section, $P_l(\mu_d)$ is the l-th Legendre polynomial in μ_d, and N is the number of discrete directions considered. Multidimension parallels exist, are very similar in nature to the slab equations, and are omitted for brevity here. It is important to note that since for many cases $L << N-1$ the $\mathbf{S\Psi}$ operator is low rank. Typically this is taken advantage of by storing only the moments of the angular flux in memory, not the full $\mathbf{\Psi}$ vector.

A standard S_N solution technique to solve the above equation is source iteration (SI), where the angular redistribution term has been lagged:

$$\mathbf{L}\Psi^{m+1} = \mathbf{S}\Psi^{m} + q = Q\,. \tag{4.5}$$

Due to the collocative nature of the discrete ordinates technique, $\mathbf{L}$ can be inverted one angular direction at a time (in some situations with reflective boundary conditions, directions can be coupled but the typical approach is to lag this coupling as

well). Furthermore, for a given direction, the spatial solve can be carried out on a direct cell-by-cell basis due to the upwind character of the spatial discretizations used. This solution of Eq. (4.5) is typically referred to as a transport sweep.

4.2 Nonlinear Source Iteration

All of the nonlinear methods we have considered render the streaming operator $\mathbf{L}$ nonlinear, i.e., $\mathbf{L\Psi} \rightarrow \hat{\mathbf{L}}(\mathbf{\Psi})$, yielding the nonlinear system $\hat{\mathbf{L}}(\mathbf{\Psi}) - \mathbf{S\Psi} = q$ at each source iteration. One possible approach would be to solve the nonlinear system by inverting $\hat{\mathbf{L}} - \mathbf{S}$ via a Newton solve at the expense of keeping the entire solution vector $\mathbf{\Psi}$ in memory as compared to the low rank $\mathbf{S\Psi}$ operator. In order to avoid this expense, we have opted to solve the nonlinear problem in each individual cell during a transport sweep in a given direction, with a fixed right-hand-side source term stemming from the previous source iteration (i.e., standard SI). Solution of the 2×2 (slab geometry) and 3×3 nonlinear system of equations is not too costly since the systems being solved are quite small. Specific information regarding $\widetilde{\psi}$ within cell i for direction d is not retained between source iterations m and $m+1$. Therefore $\widetilde{\psi}$ is found anew for each direction d, within cell i, for every source iteration m. This enables us to avoid saving the full angular flux vector across source iterations unless $\mathbf{S\Psi}$ is full rank.

4.3 Commonalities of SI for All Methods Considered

Convergence of the source iteration process is based on the normalized change in the cell average scalar flux, $\Delta\phi_{A,i,l}$:

$$\Delta\phi_{A,i}^{\ell} = \frac{|\phi_{A,i}^{\ell} - \phi_{A,i}^{\ell-1}|}{|\phi_{A,i}^{\ell}|} \,. \tag{4.6}$$

Iteration is stopped on the condition that:

$$\max_{1 \leq i \leq N_{cells}} \left[\frac{|\phi_{A,i}^{\ell} - \phi_{A,i}^{\ell-1}|}{|\phi_{A,i}^{\ell}|} \right] \leq 10^{-6} \,. \tag{4.7}$$

4.4 Solving for $\widetilde{\psi}$ in a Single Cell for Direction d

4.4.1 LD Specific

The LD definitions of $\psi_{A,i}$, $\psi_{X,i}$, and $\psi_{i+1/2}$, when inserted into Eqs. (2.5) creates a linear system of equations from which the two unknowns of $\widetilde{\psi}_{LD}$, a_{LD} and b_{LD} can be directly solved with a single matrix inversion, thus giving the angular flux solution for direction d within a single celll for the latest scattering source iterate. Similarly in rectangular geometry, when the LD representation is used to close Eq. (3.7), a 3×3 linear system of equations from which the unknowns a_{LD}, b_{LD}, and c_{LD} can be directly solved giving $\widetilde{\psi}_{LD}$ for direction d in a single cell.

4.4.2 ED Specific

Applying the ED definitions to Eqs. (2.5) always forms a nonlinear system of equations that describes $\widetilde{\psi}_{ED}$ within cell i for direction d. The initial trial parameters, c_1 and c_2, are found by linearly expanding the definitions of Eq. (2.13a), Eq. (2.13b), and Eq. (2.13c) about an arbitrary pair of iterates, c_{1*} and c_{2*}, and taking the limit as $c_{2*} \to 0$, yielding the following definitions:

$$\psi_{i+1/2} = e^{c_{1*}} + (c_1 - c_{1*})e^{c_{1*}} + c_2 e^{c_{1*}}\,, \tag{4.8a}$$

$$\psi_A = e^{c_{1*}} + (c_1 - c_{1*})e^{c_{1*}}\,, \tag{4.8b}$$

$$\psi_X = c_2 e^{c_{1*}}\,. \tag{4.8c}$$

Inserting Eq. (4.8) directly into Eq. (2.5) yields a linear system of equations in terms of unknowns c_1 and c_2, giving a reasonable first iterate to begin the nonlinear search for c_1 and c_2 that satisfy the full moment equations. Satisfactory c_1 and c_2 are found using Newton's method with an analytically formed Jacobian.

4.4.3 CSZ Specific

Working as a modification of the LD solution, the initial trial for CSZ was the LD solution, $\widetilde{\psi}_{LD} = \hat{\psi}_{csz}$. If $\hat{\psi}_{csz} \geq 0$ everywhere within a cell, $\widetilde{\psi}_{LD} = \widetilde{\psi}_{csz}$. Otherwise, this first iterate of $\hat{\psi}$ was used and the nonlinear CSZ definitions for the unknowns of Eqs. (2.5) or Eqs. (3.7) were applied (as appropriate to the geometry), and Newton's method with an analytical Jacobian was used to solve the resultant set of nonlinear equations. CSZ has an everywhere defined Jacobian, but the Jacobian is discontinuous. Nonetheless, Newton iteration worked in all of our test problems. Similar results concerning a discontinuous Jacobian have been observed by Fichtl, et al. [6].

4.4.4 ED and CSZ Commonalities

To minimize the number of iterations required for cell convergence, undamped Newton iteration (step length = 1) was always used initially to solve the nonlinear set of equations generated with either ED or CSZ. However, if the search for the ED or CSZ parameters that describe $\widetilde{\psi}$ began to take too long (lots of iterations), indicating that Newton's method was beginning to diverge, the iteration was reset to the initial guess, and the step length parameter reduced. More sophisticated nonlinear search techniques, such as the minimization of the residual formed by moment equations, as suggested in [17] were attempted. However it was observed that these techniques quite frequently found a localized, but not global minimum of the moment equations residuals, effectively failing to find a solution. Thus, the more sophisticated techniques were abandoned, and the crude, but effective iteration duration based step length adjustment system was used. It was more desirable to have convergence to the true solution rather than efficiently finding the incorrect solution.

To assure the same level of convergence, ED and CSZ convergence was based on the normalized change of $\psi_{A,i,d}$ within cell i between Newton iterations n and $n-1$:

$$\frac{|\psi^n_{A,i,d} - \psi^{n-1}_{A,i,d}|}{|\psi^n_{A,i,d}|} \leq 10^{-8}\,, \tag{4.9}$$

where i refers to cell i in slab geometry or cell i,j in rectangular geometry.

4.4.5 WL Specific

To find $\widetilde{\psi}_{WL}$, the WL scheme begins by first finding $\widetilde{\psi}_{LD}$ by inverting a 3×3 matrix and checking the calculated outflow for positivity. If $\widetilde{\psi}_{LD}$ is positive along the entire outflow of cell i,j, then $\widetilde{\psi}_{LD} = \widetilde{\psi}_{WL}$. Otherwise, a second matrix inversion is required to solve the WL linear equations (*not* the moment equations) appropriate to correcting the number of negative vertices associated with $\widetilde{\psi}_{LD}$. After the 2nd matrix inversion, the WL scheme is complete, having found $\widetilde{\psi}_{WL}$ within cell i,j for direction d.

4.5 Estimating the Relative Computational Cost

To measure the relative computational costs of each method, we consider the number of matrix inversions required to solve a problem. As LD is computationally the simplest and cheapest, we normalize the total number number of matrix inversions required by ED, CSZ, and WL to uniformly converge the source iteration, Eq. (4.7) to the total number of LD matrix inversions required to reach the same convergence. It must be emphasized that LD, ED, CSZ, and WL do not necessarily require the same number of source iterations to converge a problem.

LD requires a single matrix inversion for each direction, in every cell, for each source iteration. For ED and CSZ, the number of matrix inversions is equal to the cumulative total of all first iterate formations (requires a matrix inversion) and Newton iterations required for every cell (inversion of the Jacobian matrix), required to

solve the nonlinear system of equations formed for every direction, in each cell, until the scattering source is converged. WL will require at most two matrix inversions for each cell, direction, and source iteration. Admittedly, there is a nontrivial additional amount of computational work required for ED and CSZ to calculate the respective nonlinear quantities required to solve the moment equations for a single Newton iteration, however, a rough estimate of the amount of work required for each method can be obtained by comparing matrix inversions.

5. SLAB GEOMETRY COMPUTATIONAL RESULTS

5.1 Comparison of Theoretical Outflow and Slope Values for LD, ED, and CSZ Schemes

The fundamental differences between the LD, ED, and CSZ schemes are best illustrated by comparing the normalized outflow values calculated by each method given the value of ψ_A and ψ_X. Fig. 5.1 shows the outflow for LD, CSZ, and ED for $\mu > 0$.

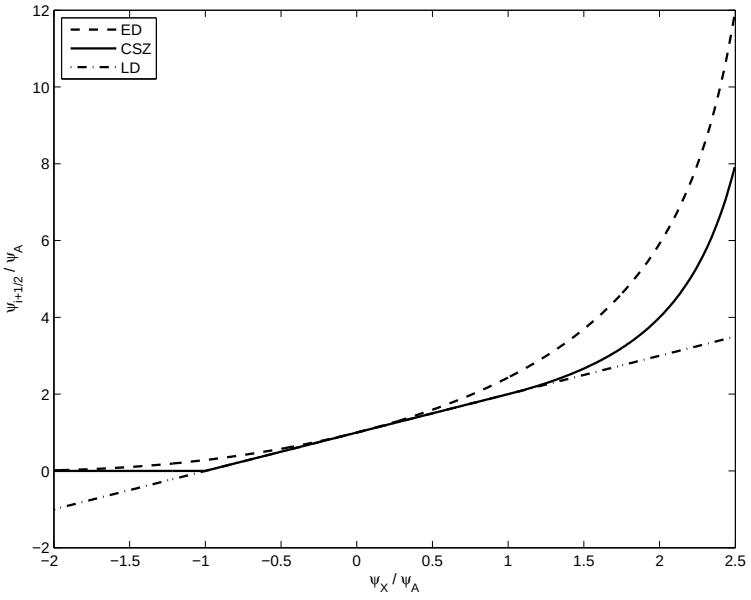

Fig. 5.1. Slab geometry comparison of LD, ED, and CSZ outflows for $\mu > 0$.

Theoretically, $\frac{\psi_X}{\psi_A} \in [-3, +3]$. However $\frac{\psi_X}{\psi_A}$ is restricted to $\frac{\psi_X}{\psi_A} \in [-2, +2.5]$ to illustrate the more subtle variations between LD, ED, and CSZ in the more commonly observed regime near $\frac{\psi_X}{\psi_A} = 0$. LD maintains a linear trend over the range $-3 \leq \frac{\psi_X}{\psi_A} \leq +3$. The outflow plot of Fig. 5.1 demonstrates several key points:

1. both ED and CSZ are strictly positive, and LD can yield outflows < 0,

2. both ED and CSZ follow the limit:

$$\lim_{\frac{\psi_X}{\psi_A} \to +3} \left[\frac{\psi_{i+1/2}}{\psi_A} \right] = \infty \,, \tag{5.1}$$

3. both ED and CSZ follow the limit:

$$\lim_{\frac{\psi_X}{\psi_A} \to -3} \left[\frac{\psi_{i+1/2}}{\psi_A} \right] = 0 \,, \tag{5.2}$$

4. CSZ yields the LD solution exactly when the LD solution is everywhere positive within the cell,

5. CSZ is *always* closer to the LD solution than is ED.

5.2 Slab Test Problem 1- Pure Absorber

Our first slab geometry test problem again illustrates the strictly positive nature of the new CSZ method as compared to the negativities associated with LD and optically thick cells in slab geometry. Fig. 5.2 shows the results of a pure absorber problem, with total slab width of 12 cm, $\sigma_t = \sigma_a = 1\text{cm}^{-1}$, using S_8 angular quadrature, with 3 uniform spatial cells. The left boundary condition is an isotropic incident flux, normalized to yield a unit current; the right boundary condition is a vacuum boundary. Average scalar flux of a given cell is plotted at the midpoint of the cell.

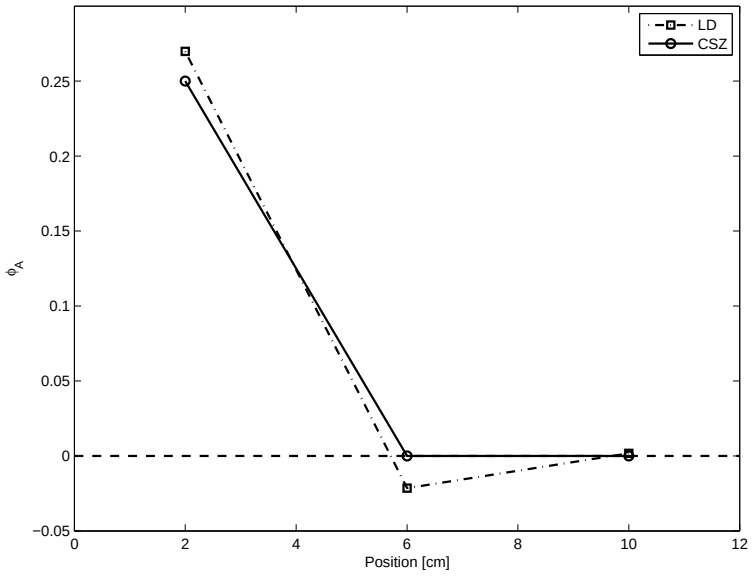

Fig. 5.2. Slab test problem 1 average scalar flux comparison of LD and CSZ for a strong absorber with thick cells.

For the same absorber problem, we show a convergence rate plot for LD and CSZ in Fig. 5.3. Error is taken as the L_2 difference between the numerically calculated scalar flux average, $\phi_{A,num,i}$, and the analytically calculated $\phi_{A,i,exact}$ as shown by Eq. (5.3):

$$Error = \sqrt{\sum_{i=1}^{N_{cells}} \left[\Delta x_i \left(\phi_{A,ex,i} - \phi_{A,num,i}\right)^2\right]}, \tag{5.3a}$$

$$\phi_{A,ex,i} = \sum_{d=1}^{N_{dir}} \left[\frac{1}{\Delta x_i} \int_{x_i-1/2}^{x+1/2} \left[w_d \psi_{0,d} e^{-\Sigma_A x/\mu_d}\right]\right], \tag{5.3b}$$

$$\phi_{A,num,i} = \sum_{d=1}^{N_{dir}} w_d \psi_{A,d,i}\,. \tag{5.3c}$$

Eq. (5.3b) is valid for the case of a pure absorber for all ordinates d, with direction cosines of μ_d, with weights w_d that sum to 1, and incident angular flux (at the slab boundary) of $\psi_{0,d}$.

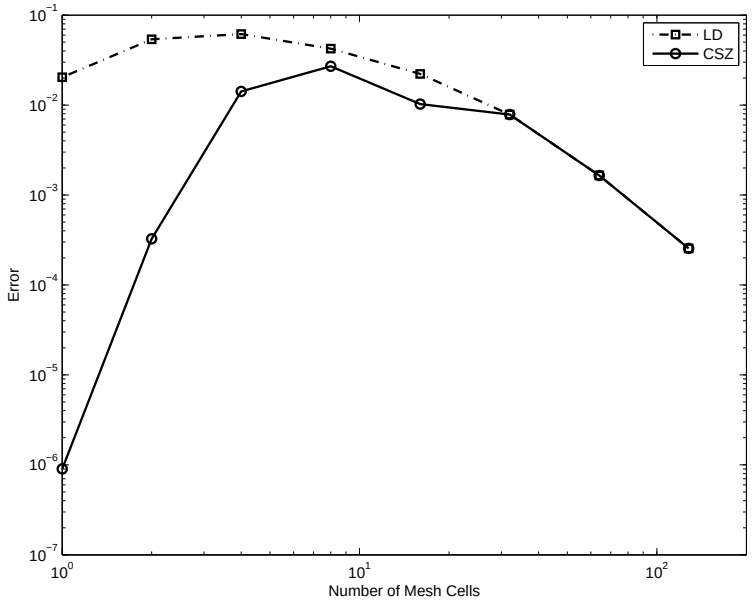

Fig. 5.3. Slab test problem #1 LD and CSZ rate of convergence plot.

Fig. 5.3 shows that in addition to being strictly positive, CSZ is also more accurate than is LD on coarse meshes, and that as the mesh is refined, CSZ becomes equivalent to LD so the order of convergence of CSZ is as high as LD. It must be noted that ED calculates the exact solution in a purely absorbing medium, thus it is omitted from Fig. 5.3.

5.3 Slab Test Problem 2- Slab with $c = 0.5$

The next two test cases employ an S_8 angular quadrature and a 12 cm wide homogeneous slab. Slab test problem 2 consists of an isotropic, left incident, unit current angular flux, vacuum boundary conditions on the right face, no distributed source, $\sigma_t = 1\text{cm}^{-1}$, and $c = 0.5$. To calculate the reference solution, the analytic scalar flux solution provided in [18] was used. $\phi_{A,ex,i}$ was calculated not by direct integration, as in Eq. (5.3b) but rather by using 2 point Gauss integration to estimate

$\phi_{A,i}$ over the interval $[x_{i-1/2}, x_{i+1/2}]$. Total error was then calculated in the same manner as in Eq. (5.3a).

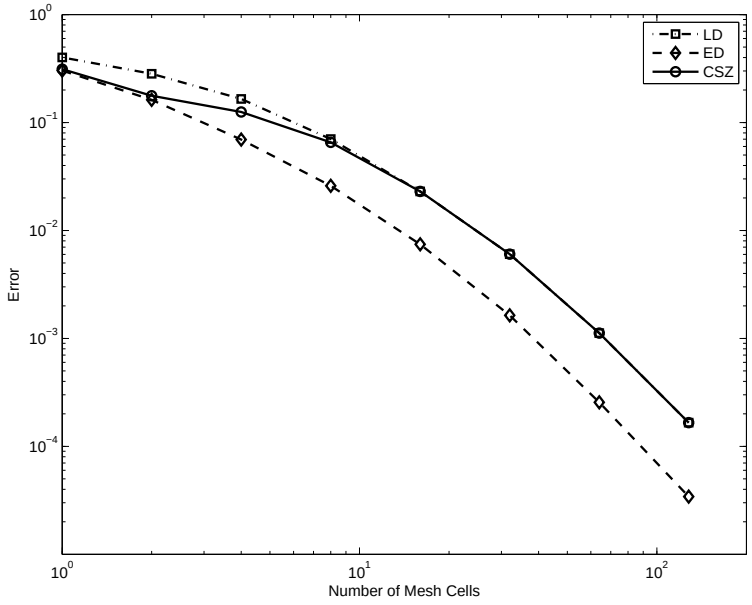

Fig. 5.4. Slab test problem 2 order of convergence.

Fig. 5.4 shows that ED is more accurate than both LD and CSZ. However, Fig. 5.4 also shows that LD,CSZ, and ED all have the same order of accuracy as the mesh is refined. The accuracy of ED relative to that of LD and CSZ is a problem dependent phenomena as shown by the final slab problem.

5.4 Slab Test Problem 3- Slab with Distributed Source

Slab test problem 3 is similar to the first two problems, but with vacuum boundary conditions on both faces, an isotropic unit source distributed throughout the slab, $\sigma_t = 1\text{cm}^{-1}$, and $c = 0.9$. It should be noted that CSZ is in fact plotted in Fig. 5.5, but that the problem is such that LD does not produce any negativities except as the mesh becomes extremely fine. On fine meshes (32 cells or more) LD does in fact

produce negative angular flux solutions in boundary cells for some skimming incident angles. However, these negativities are small, occur only in the outermost boundary cells, occur only for a directions, and converge to 0 with further cell refinement, thus LD and CSZ produce either identical or nearly identical results as shown by Fig. 5.5.

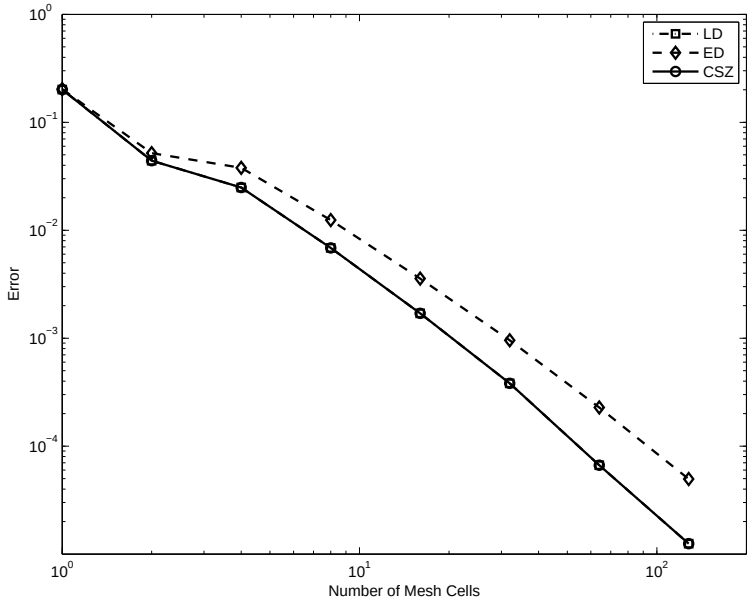

Fig. 5.5. Slab test problem 3 convergence rates.

It is clear from Fig. 5.5 that the ED method is less accurate than both LD and CSZ for the distributed source problem. This is in contrast with slab test problem 2 and is presumably due to the fact that ED has the wrong sign of curvature for the distributed source problem. This ED effect is consistently seen for problems with negative curvature, like slab test problem 3.

5.5 Slab Computational Costs

The computational costs for the 3 slab test problems are listed in Table 5.1, Table 5.2, and Table 5.3.

Table 5.1
Number of matrix inversions required for the ED and CSZ methods relative to LD for a pure absorber slab (slab test problem #1).

Number of Cells	Method	
	ED	CSZ
1	5.63	6.63
2	5.50	3.31
4	5.63	1.91
8	7.78	1.14
16	5.00	1.06
32	4.76	1.00

Table 5.2
Number of matrix inversions required for the ED and CSZ relative to LD for a homogeneous slab with a scattering absorber (slab test problem #2).

Number of Cells	Method	
	ED	CSZ
1	10.93	11.36
2	14.03	4.94
4	11.47	4.44
8	13.14	1.32
16	11.12	1.02
32	10.89	1.01

Table 5.3
Number of matrix inversions required for the ED and CSZ methods relative to LD for a slab with a distributed internal source (slab test problem #3).

Number of Cells	Method	
	ED	CSZ
1	6.21	1.00
2	6.45	1.00
4	6.39	1.00
8	9.55	1.00
16	6.58	1.00
32	6.32	1.04

Overall, the data of Table 5.1, Table 5.2, and Table 5.3 indicates that CSZ is generally less costly than ED, and in several cases, by initially yielding the LD solution CSZ does not even require the solution of a nonlinear system of equations. Since ED yields the exact analytic solution for a pure absorber, its convergence data was omitted from Fig. 5.3, but is present in Table 5.1 to illustrate the significant cost inherent to ED, even though $\widetilde{\psi}_{ED}$ is the exact solution for a pure absorber. The other significant trend which must be highlighted is the decrease in computational cost of the CSZ method as the mesh is refined. This trend is again a direct result of CSZ initially yielding the LD solution. As the mesh is refined, LD yields fewer and fewer negative angular fluxes, thus, CSZ modifies fewer LD solutions. The exception to this trend comes in the distributed source problem (slab test problem #3). In slab test problem #3, as the mesh is refined, LD begins to generate negative values of $\widetilde{\psi}_{LD}$ at the inflow of boundary cells for directions with $|\mu| \approx 0$. This is a result of the LD solution generating values of $\frac{\psi_X}{\psi_A} > 1$. The negativities are not too severe, being on the order of 1E-4. However since CSZ is strictly positive *everywhere* within a cell, as

the scattering source increases with the source iteration process, using CSZ requires the solution of a nonlinear set of equations, thus the increase in computational work seen in Table 5.3.

6. RECTANGULAR GEOMETRY COMPUTATIONAL RESULTS

In slab geometry, LD produces negative angular flux solutions only in optically thick cells. However, in rectangular geometry, negativities are not limited to strongly absorbing cells; negativities can be produced in void regions. We therefore present a series of test problems which are known to produce poor results when using the LD spatial discretization.

6.1 Rectangular Test Problem 1- Glancing Flux Into a Void

The first rectangular geometry test problem illustrates the negativities that can occur in voids with glancing incidence angular flux when using the LD scheme. We choose a 1cm x 1cm void with a beam of radiation incident along the bottom face in the direction $\mu = 0.90$, and $\eta = \sqrt{1-\mu^2}$.

Fig. 6.1 graphically shows the calculated angular flux representation, $\widetilde{\psi}$ on the interior of the domain for each method versus the exact analytical solution when the domain is divided into 1 cell. LD clearly propagates a significant negative outflow along the top face of the cell, while the CSZ and WL schemes produce strictly positive outflows. Of greater interest is the comparison of $\widetilde{\psi}_{CSZ}$ and $\widetilde{\psi}_{WL}$. By not conserving Eq. (3.7b) and Eq. (3.7c), WL significantly increases numerical diffusion within the cell. The implications of this increased numerical diffusion are not obvious with a single cell, but are clearly illustrated by dividing the domain into finer and finer meshes.

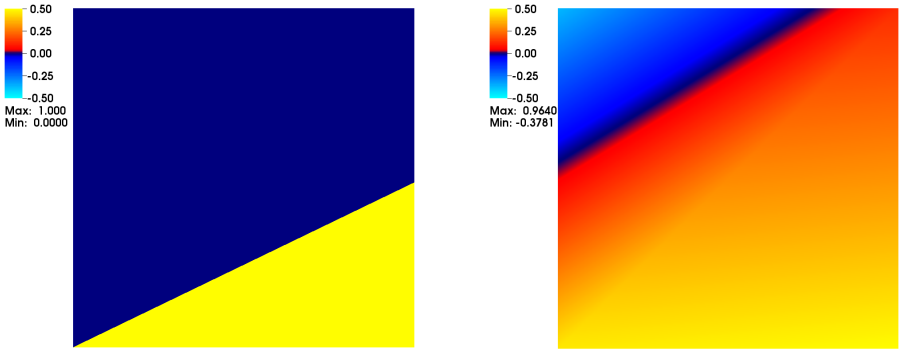

(a) Analytic

(b) LD

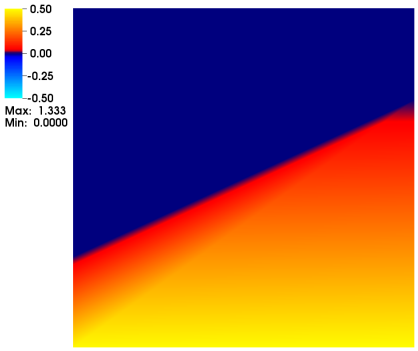

(c) CSZ

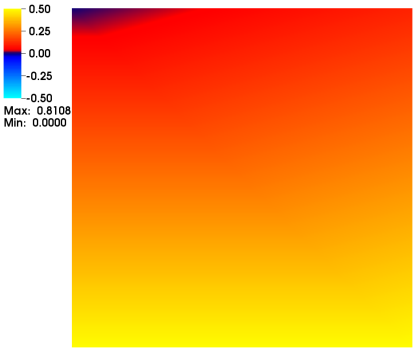

(d) WL

Fig. 6.1. Comparison of the $\widetilde{\psi}(x, y)$ calculated with each numerical scheme versus the analytic solution, $\psi(x, y)$, for rectangular test problem 1.

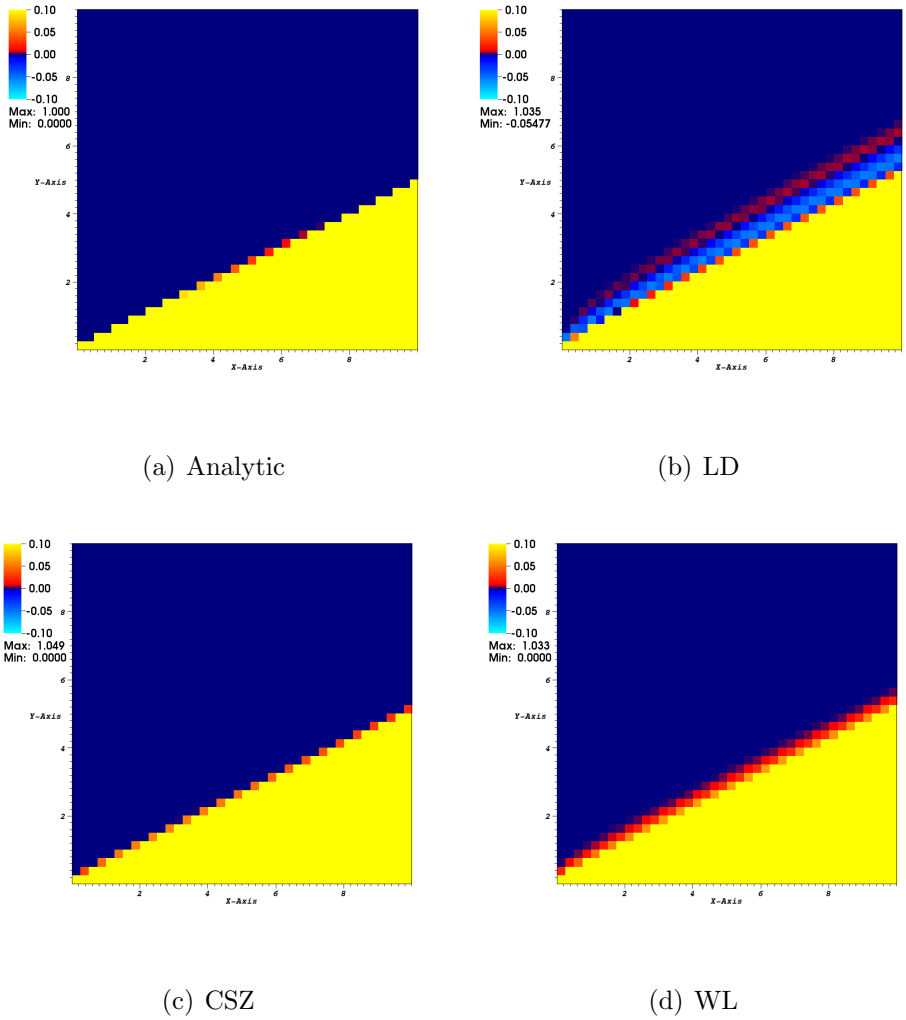

(a) Analytic (b) LD

(c) CSZ (d) WL

Fig. 6.2. Plots of $\psi_{A,i,j,d}$ for the discretized void problem (rectangular test problem 1). Linear plot scale to illustrate negativities and oscillations of LD.

Figure 6.2 shows a linear scale plot of the analytic and the numerically calculated values of $\psi_{A,i,j,d}$ when the problem is divided into 1600 total mesh cells. The analytic solution for this problem, $\psi_{ex,A,i,j,d}$, is the fraction of cell $i,\ j$ which lies below the line $y = \frac{\eta}{\mu}x$. From Fig. 6.2, it is clear the the LD solution is exhibiting two important, non-physical qualities:

1. negativities,

2. oscillations and angular flux propagation into the region where $\psi_{ex}(x, y) = 0$.

Though WL produces a strictly positive angular flux solution without any oscillations, the issue of numerical diffusion begins to seriously degrade the solution. This is apparent from the linear graph, Fig. 6.2, but Fig. 6.3 is provided to make this more apparent.

CSZ largely avoids any numerical diffusion; the strictly positive piecewise linear flux shape strongly inhibits the numerical spreading of the angular flux solution into the region where $\psi(x, y) = 0$. Looking beyond this single refinement, the L2 norm of total solution error:

$$Error = \sqrt{\sum_{i=1}^{N_{x\ cells}} \sum_{j=1}^{N_{y\ cells}} \left[\Delta x_i \Delta y_j \left(\psi_{A,ex,i,j} - \psi_{A,num,i,j}\right)^2\right]}, \tag{6.1}$$

where $N_{x\ cells}$and$N_{y\ cells}$ are respectively the number of cells in the x and y directions is plotted in Fig. 6.4.

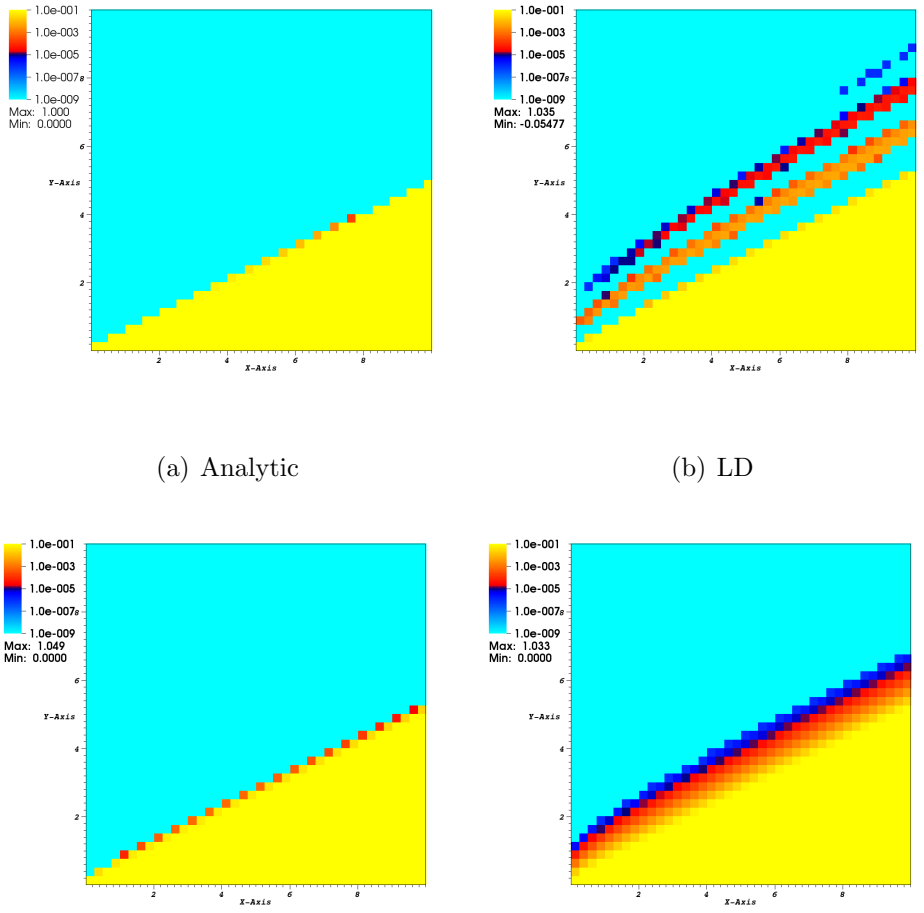

(a) Analytic (b) LD

(c) CSZ (d) WL

Fig. 6.3. Logarithmic scale plots of $\psi_{A,i,j,d}$ for the discretized void problem (rectangular test problem 1). Logarithmic scale to highlight WL numerical diffusion. Negativities and 0s are represented as the minimum of the color scale.

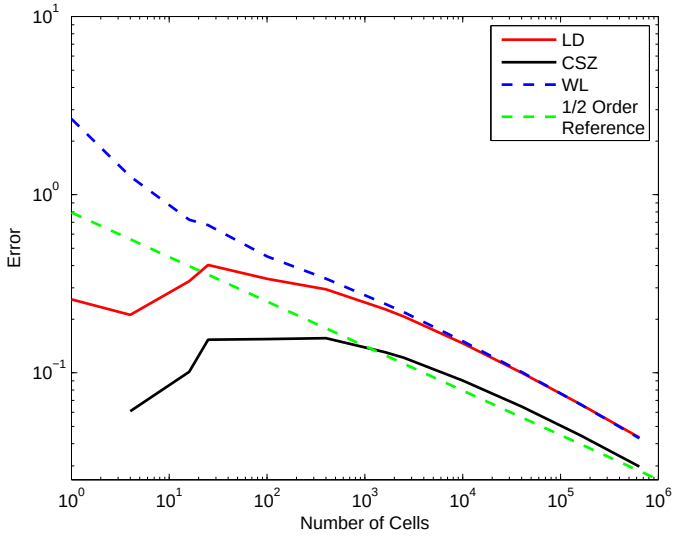

Fig. 6.4. L2 norm order of convergence plot for the large void problem (rectangular test problem 1).

Several trends are demonstrated by Fig. 6.4 for the discretized void problem:

1. CSZ is always more accurate than LD and WL,
2. all three numerical methods approach the same order of convergence, and
3. none of the three numerical methods exceed the theoretical convergence limit of 1/2 order [19].

It should be noted that CSZ yields the exact value of $\psi_{A,i,j}$ for a single cell, resulting in an error of 0 which cannot be plotted on a logarithmic scale graph, that $\widetilde{\psi_{csz}} \neq \psi$. The dashed green line in Fig. 6.4 is provided as a reference line of order 1/2 convergence rate, the theoretical maximum rate of convergence for this problem [19].

6.2 Rectangular Test Problem 2- An Iron Water Like Problem

Our next problem is similar to the classic iron water problem. As shown in Fig. 6.5, the test problem consists of a 50cm x 50cm, homogeneous rectangle, with $\sigma_t = 1.0\text{cm}^{-1}$, a scattering ratio of $c = 0.75$, and an isotropic source in the lower left 10cm x 10cm corner of the problem, with an average source strength, S_A, of 1 $\left[\frac{\text{n}}{\text{cm}^2\ \text{s}}\right]$. The bottom and left boundaries are reflective, while the top and right boundaries are vacuum. The problem was discretized with a uniform spatial discretization, $\Delta x_i = \Delta y_j$, with a total mesh size varying between 25-6400 cells, using a level-symmetric S_8 angular quadrature. The total reaction rate within three, 10cm x 10cm square regions, denoted $R1$, $R2$, and $R3$ respectively, as shown in Fig. 6.5, were calculated.

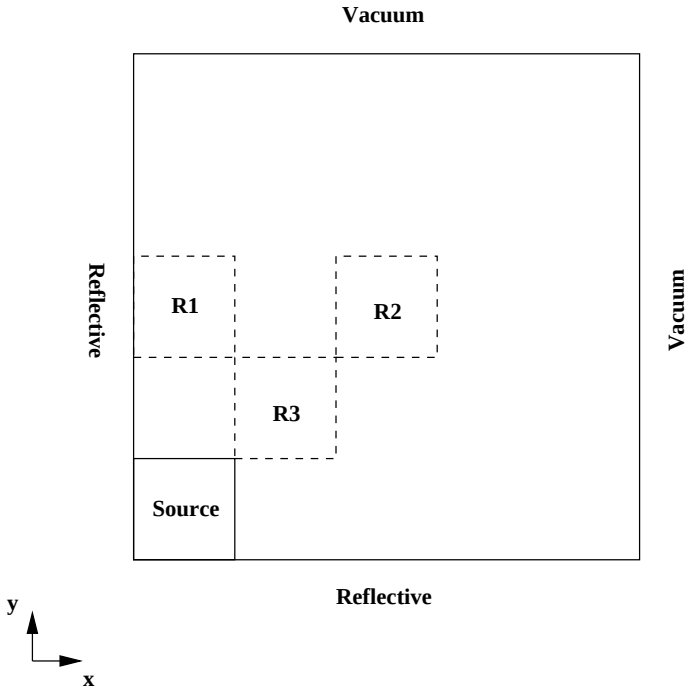

Fig. 6.5. Diagram of rectangular test problem 2 with the location of the three regions, $R1$, $R2$, and $R3$.

Plots of the reaction rate within each each region of interest are plotted in Fig. 6.6, Fig. 6.7, and Fig. 6.8.

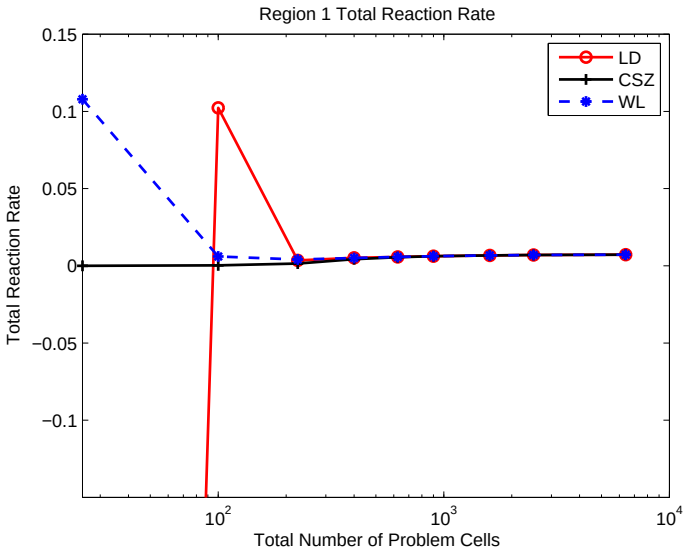

Fig. 6.6. Total reaction rates for each method in $R1$ of the rectangular test problem 2.

As the mesh is refined, LD, WL, and CSZ should converge to the same reaction rate within each region, as seen qualitatively in Fig. 6.6, Fig. 6.7, and Fig. 6.8. The reference used to compute quantitative values of error is a very fine LD mesh solution that used 25600 cells. This fine mesh solution was then collapsed appropriately, and the L2 norm of the difference between the coarse mesh solution and the collapsed fine mesh solution were used to compute error.

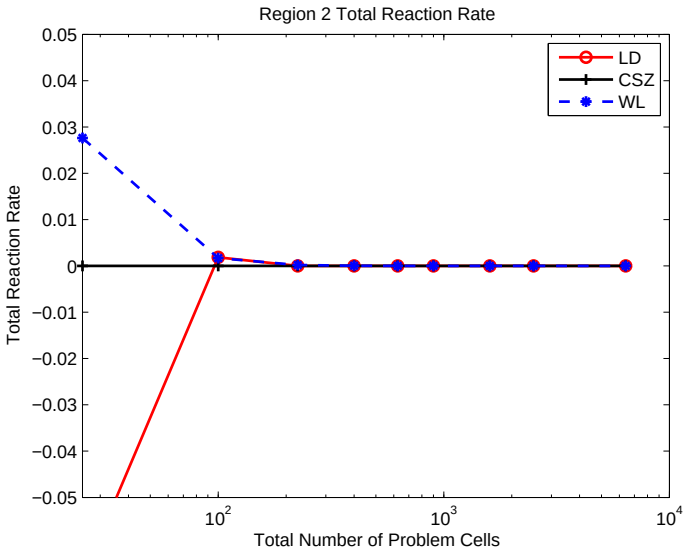

Fig. 6.7. Total reaction rates for each method in $R2$ of rectangular test problem 2.

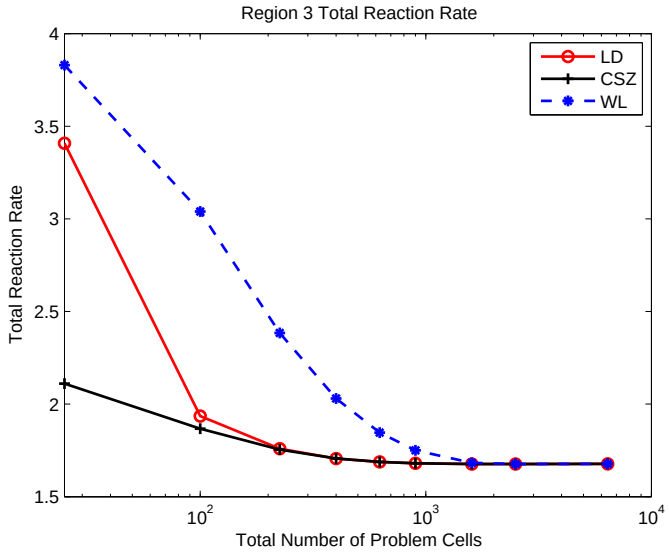

Fig. 6.8. Total reaction rates for each method in $R3$ of rectangular test problem 2.

Figures 6.6, 6.7, and 6.8 indicate several important trends:

1. WL and CSZ are always non-negative,
2. WL and CSZ converge to the LD solution,
3. LD can calculate significant negativities,
4. LD is subject to oscillations,
5. CSZ coarse mesh calculations are significantly more accurate than LD or WL solutions on the same mesh, and
6. WL can be significantly less accurate than LD (see Fig. 6.8).

6.3 Rectangular Test Problem 3- Beam Bending Examination

In [20] Mathews examined the ability of various spatial discretizations to accurately propagate angular flux beams in the correct direction. Mathews performed his testing using a purely absorbing medium with angular flux incident on only one face in a mono-directional, thin beam. In a purely absorbing or pure vacuum medium that is free of internal sources, the exact angular flux solution propagates only in those directions which have incident angular flux. However, in Mathews analysis [20], it was shown that several spatial discretizations commonly used for discrete ordinates calculations actually produce solutions in which the angular flux solution travels in the wrong direction in a purely absorbing problem. To examine the capability of the

CSZ scheme for propagating angular flux in the correct direction, we consider a test problem consisting of a 10 cm x 10 cm void with a 1cm wide beam of incident radiation along the bottom face of the region only in the direction of $\mu = 0.5,\ \eta = \frac{\sqrt{3}}{2}$. The angular flux solution calculated along the top face of the problem ($y = 10$cm) by all three numerical schemes, as well as the analytic solution is shown in Fig. 6.3 for $\Delta x_i = \Delta y_j = 0.2$cm.

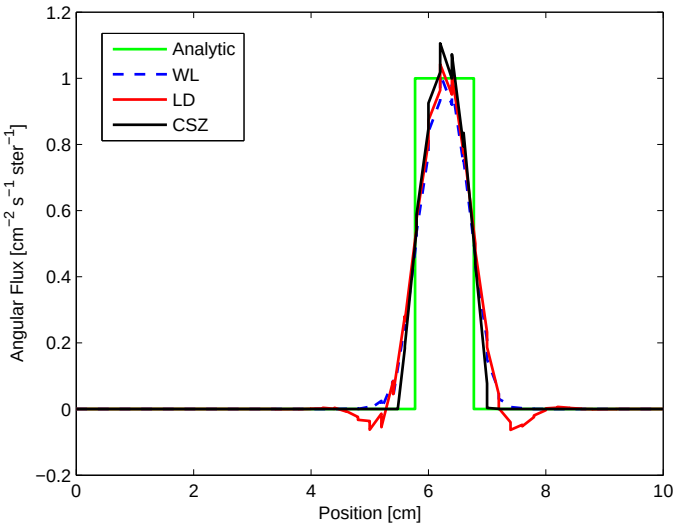

Fig. 6.9. Angular flux solution along $y = 10$cm face of rectangular test problem 3.

Results from other resolutions, both coarser and finer, display essentially the same behavior: CSZ is closer to the analytic solution than WL or LD, but the amount of bending is essentially the same for all numerical schemes examined here. This result is consistent with the results of Mathews: the LD scheme does bend the angular flux solution into the wrong direction, but the LD bending effect is not that significant.

6.4 Rectangular Computational Costs

The benefits of WL, requiring at most 2 matrix inversions to provide a strictly positive angular flux solution, is obvious when considering the first entry of Table 6.1. In the single cell void, there is only 1 cell with 1 direction that requires a strictly

Table 6.1
Number of matrix inversions relative to LD in a rectangular void versus number of cells.

Number of Cells	Method	
	CSZ	WL
1	8	2
4	4.75	1.75
16	2.69	1.75
25	2.80	1.76
100	1.99	1.74
400	3.07	3.15
1.6K	1.28	1.32
2.5K	1.23	1.26
10K	1.11	1.13
40K	1.05	1.07
160K	1.03	1.03
640K	1.01	1.02

non-negative modification. As expected, WL requires 2x more work than LD. CSZ requires multiple Newton iterations, and thus does 8x more work than LD. However, Table 6.1 also clearly illustrates the computational costs associated with the numerical diffusion of WL. If CSZ and WL were applied in the same number of cells in the large void problems, we would expect to maintain the single cell ratio of

4x more computational work for CSZ than WL. However, this is obviously not the case. By numerically diffusing the incident angular flux, many more cells require a modification of the LD solution to eliminate the negativities associated with $\widetilde{\psi}_{LD}$.

In the large void, we considered only the costs of CSZ and WL. However, cost is not a complete tool for evaluating a method, the costs and benefits of a method must be considered together. One way to quantify this would be to consider the relative efficiency of each method. Defining a quantitative measure of efficiency as:

$$\text{Efficiency} = \frac{1}{\text{Error} \times \text{Work}} \tag{6.2}$$

we examine the relative computational efficiency of LD, WL, and CSZ in each region considered for rectangular test problem 2. Fig. 6.10, Fig. 6.11, and Fig. 6.12, show plots of the efficiency for R1, R2, and R3 respectively.

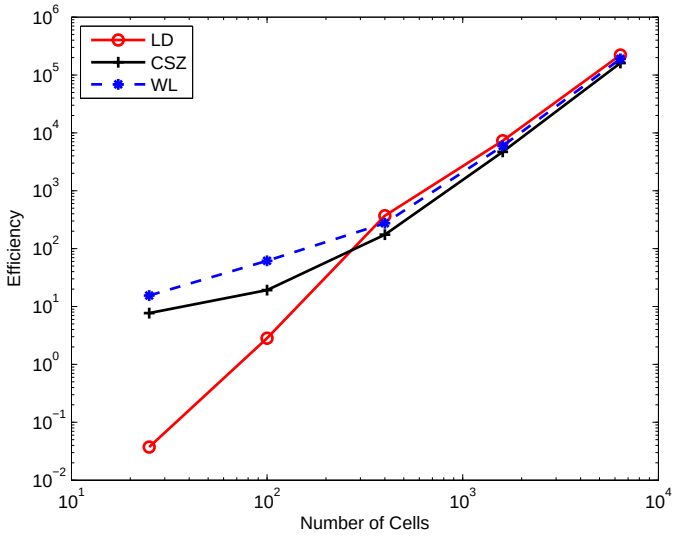

Fig. 6.10. Relative computational efficiency of each method for R1 of rectangular test problem 2.

The efficiency plots for rectangular test problem 2 demonstrate that though the CSZ method can be more computationally costly, the cost is offset by increased

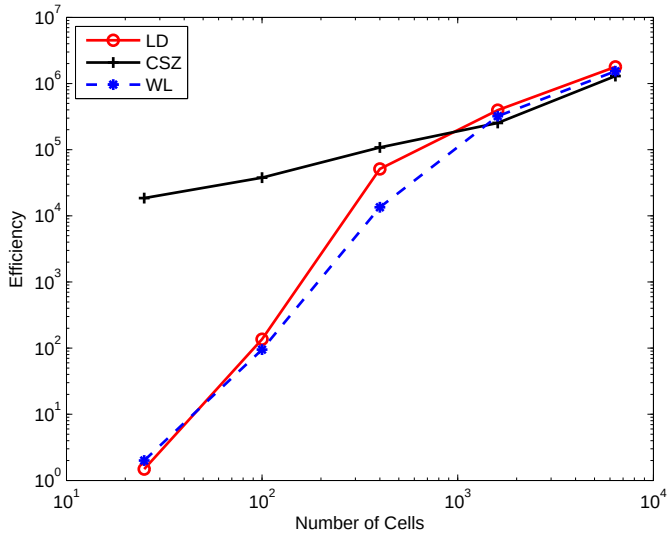

Fig. 6.11. Relative computational efficiency of each method for R2 of rectangular test problem 2.

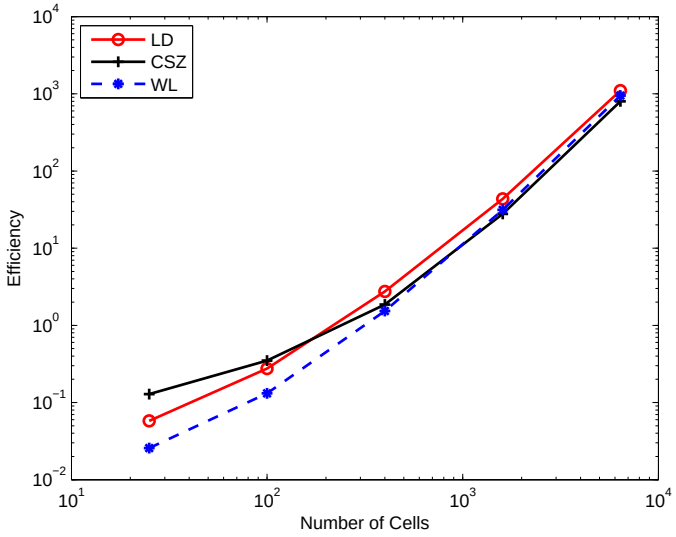

Fig. 6.12. Relative computational efficiency of each method for R3 of rectangular test problem 2.

accuracy. CSZ is generally more efficient than both LD and WL, and depending on the problem, can be several orders of magnitude more efficient than LD or WL as shown in Fig. 6.10 and Fig. 6.11. When less efficient that LD or WL, the CSZ method is still very close in efficiency to the other methods as demonstrated by Fig. 6.12.

7. CONCLUSIONS

The CSZ scheme has been derived for slab and rectangular geometries. By design, CSZ is a nonlinear modification of the LD scheme. As such, CSZ bridges the gap between the traditional ad-hoc fixups and inherently positive solutions such as ED. Unlike previous techniques derived to yield inherently positive solution representations, CSZ is designed to differ from LD only when the LD solution is not everywhere positive within a cell. Though ad-hoc fixups also exhibit this characteristic, ad-hoc fixups do not conserve the zeroth and linear spatial moments of the transport equation, which CSZ always preserves. We have shown that by defining $\widetilde{\psi}_{csz}$ as a linear function with all negativities set-to-zero, that the zeroth and linear moments of the transport equation can be used to uniquely determine the unknowns which completely describe $\widetilde{\psi}_{csz}$. More specifically, there is a unique $\widetilde{\psi}_{csz}$ given any physically valid set of spatial moments. If LD is everywhere positive within a cell, the equations describing $\widetilde{\psi}_{csz}$ are linear. Otherwise, the moment equations form a nonlinear system of equations. If LD is not everywhere positive, ad-hoc fixups use auxiliary equations, not the moment equations to determine $\widetilde{\psi}$.

Test problems in slab geometry indicate that:

1. CSZ is always everywhere positive for the physically realizable range of $\frac{\psi_X}{\psi_A}$,
2. CSZ is always closer to the LD solution than ED,
3. CSZ converges at the same rate as LD and ED,
4. CSZ is at least as accurate as LD in those problems where ED is significantly less accurate than LD.

Further, the computational work associated with CSZ decreases significantly with mesh refinement, whereas the amount of work associated with using the ED scheme remains significantly higher than the work required to use LD, regardless of mesh

refinement. In general, as the mesh is refined, the LD solution becomes everywhere positive more frequently. Consequently, CSZ has to perform fewer and fewer nonlinear iterations since $\widetilde{\psi}_{csz} = \widetilde{\psi}_{LD}$ when $\widetilde{\psi}_{LD}$ is everywhere positive within a cell, but ED always has to solve a computationally intensive, nonlinear set of equations.

In rectangular geometry, CSZ was compared to a rectangular an ad-hoc fixup scheme inspired by the triangular mesh work presented by Warsa. Again, CSZ eliminated the negativities associated with LD, even in void regions. Though CSZ was significantly more expensive than the ad-hoc fixup scheme on coarse meshes, problems with more refined meshes showed that CSZ compensated for the increase in work required to find a single solution by inhibiting numerical diffusion. On finer meshes, the ad-hoc fixup technique needed to be applied more often due to numerical diffusion, both in voids and non-voided problems, negating its advantages. Our results in the iron-water like problem also showed that an ad-hoc fixup can be significantly less accurate than LD, whereas CSZ is always as accurate as LD, if not more so.

The CSZ scheme presented herein is easily extensible to 3 dimensional Cartesian (brick) geometry. Since it works as a modification of the LD scheme, CSZ can easily be incorporated into existing codes that already have cell centered LD implementations. Additional work in the areas of acceleration techniques and development of a multi-dimensional method that maintains the diffusion limit will be required for certain application areas such as radiative transfer. However, S_N codes used for radiation shielding problems can gain the most immediate benefit from implementing the CSZ scheme. CSZ will be a valuable addition to any currently existing codes that require strictly positive angular flux solution techniques.

REFERENCES

[1] E. E. Lewis and W. F. Miller. Computational Methods of Neutron Transport. American Nuclear Society, La Grange Park, IL, 1993.

[2] K. D. Lathrop. Spatial differencing of the transport equation: Positivity vs. accuracy. Journal of Computational Physics, 4 (1969) 475-498.

[3] E. W. Larsen and P. Nelson. Finite-difference approximations and superconvergence for the discrete-ordinate equations in slab geometry. SIAM Journal of Numerical Analysis, 19 (1982) 334-338.

[4] R. E. Alcouffe E. W. Larsen. The linear characterisitc method for spatially discretizing the discrete-ordinates equations in (x,y)- geometry. ANS/ENS Joint Topical Meeting, Mathematical Methods in Nuclear Engineering, Munich, FRG, April, 1981.

[5] R. E. Alcouffe, E. W. Larsen, W. F. Miller, and B. R. Wienke. Computational efficiency of numerical methods for the multigroup, discrete-ordinates neutron transport equation: The slab geometry case. Nuclear Science and Engineering, 71 (1979) 111-127.

[6] E. D. Fichtl, J. S. Warsa, and J. D. Densmore. The Newton-Krylov method applied to negative-flux fixup in S_N transport calculations. Accepted for publication in Nuclear Science and Engineering., 2010.

[7] K. Mathews, G. Sjoden, and B. Minor. Exponential characteristic spatial quadrature for discrete ordinates radiation transport in slab geometry. Nuclear Science and Engineering, 118 (1994) 24-37.

[8] B. Minor and K. Mathews. Exponential characteristic spatial quadrature for discrete ordinates radiation transport with rectangular cells. Nuclear Science and Engineering, 120 (1995) 165-186.

[9] W. F. Walters and T. Wareing. An accurate, strictly-positive, nonlinear characteristic scheme for the discrete-ordinate equations. Transport Theory and Statistical Physics, 25 (1996) 197-215.

[10] K. A. Mathews. Adaptive characteristic spatial quadratures for discrete ordinates neutral particle transport– the slab geometry case. Transport Theory and Statistical Physics, 19 (1990) 419-458.

[11] K. A. Mathews and B. M. Minor. Adaptive characteristic spatial quadratures for discrete ordinates neutral particle transport- the rectangular cell case. Transport Theory and Statistical Physics, 22 (1993) 655-685.

[12] T. A. Wareing. An exponential discontinuous scheme for discrete-ordinate calculations in cartesian geometries. Joint International Conference on Mathematical Methods and Supercomputing for Nuclear Applications. Saratoga Springs, NY, Oct. 1997.

[13] P. Maginot, J. Morel, and J. Ragusa. A positive non-linear closure for the S_N equations with linear discontinuous differencing. Proceedings of the International Conference on Mathematics, Computational Methods, and Reactor Physics (M&C 2009), Saratoga Springs, NY, May 2009.

[14] R. Vichnevetson. Computer Methods for Partial Differential Equations, Volume 1 of Elliptic Equations and the Finite-Element Method. Prentice Hall, Inc. 1981.

[15] MATLAB. Version 7.10.0.499 (2007a). From The MathWorks, Inc., Natick, MA.

[16] S. Hamilton, M. Benzi, and J. Warsa. Negative flux fixups in discontinuous finite element S_N transport. Proceedings of the International Conference on Mathematics, Computational Methods, and Reactor Physics (M&C 2009). Saratoga Springs, NY, May 2009.

[17] J. Nocedal and S. J. Wright. Numerical Optimization. Springer Science + Business Media, LLC., New York, NY, 2000.

[18] J. S. Warsa. Analytical S_N solutions in heterogeneous slabs using symbolic algebra computer programs. Annals of Nuclear Energy, 294 (2002) 851-874.

[19] C. Johnson and J. Pitkaranta. Convergence of a fully discrete scheme for two-dimensional neutron transport. SIAM Journal on Numerical Analysis, 20 (1983) 951-966.

[20] K. A. Mathews. On the propagation of rays in discrete ordinates. Nuclear Science and Engineering, 132 (1999) 155-180.

APPENDIX A
CSZ EQUATIONS

CSZ in Slab Geometry

If the CSZ scheme falls into case 3 within cell i, that is if $\widetilde{\psi}_{csz}(s) > 0$ only on $s \in [s_z, 1]$, the unknown cell quantities $\psi_{A,i,d}$ and $\psi_{X,id}$ are:

$$\psi_{A,i,d} = (1 - s_z)(a_{csz} + b_{csz} s_z)\,, \tag{A.1}$$

$$\psi_{X,i,d} = (1 - s_z)\left(b_c sz + s_z(3a_c sz - 2b_{csz}(1 - 2s_z))\right)\,. \tag{A.2}$$

CSZ in Rectangular Geometry

Edge $i, j + 1/2$ Quantities

If the CSZ scheme falls into case 3 along the edge $i, j+1/2$, that is if $\widetilde{\psi}_{csz}(s, 1) > 0$ only on $s \in [s_z, 1]$, the unknown edge quantities $\psi_{i,j+1/2,d}$ and $\psi_{M,i,j+1/2,d}$ are:

$$\psi_{i,j+1/2,d} = -\left(s_z - 1\right)\left(a_{csz} + c_{csz} + b_{csz} s_z\right)\,, \tag{A.3}$$

$$\psi_{M,i,j+1/2,d} = -(s_z - 1)\left(b_{csz}\left(1 + 2s_z(2s_z - 1)\right) + 3s_z(a_{csz} + c_{csz})\right)\,. \tag{A.4}$$

Edge $i + 1/2, j$ Quantities

Now consider edge $i + 1/2, j$. We first define t_z. Defined analogously to s_z on edge $i, j + 1/2$, t_z is the point along edge $i + 1/2, j$ where $\psi(\hat{1}, t) = 0$:

$$t_z = \frac{1}{2}\left(1 - \frac{a_{csz} + b_{csz}}{c_{csz}}\right)\,. \tag{A.5}$$

With this, we consider case 2 on edge $i + 1/2, j$, $\widetilde{\psi}_{csz}(1, t) > 0,\ t \in [0, t_z]$. For this case, the edge unknowns are:

$$\psi_{i+1/2,j,d} = t_z\left(a_{csz} + b_{csz} - c_{csz}\left(t_z - 1\right)\right)\,, \tag{A.6}$$

$$\psi_{M,i+1/2,j,d} = t_z \left(3\left(c_{csz} - b_{csz} - a_{csz}\right) + 3t_z\left(a_{csz} + b_{csz} - 2c_{csz}\right) + 4c_{csz}t_z^2\right) . \quad \text{(A.7)}$$

For case 3, $\widetilde{\psi}_{csz}(1,t) > 0,\ t \in [t_z, 1]$ the unknowns along edge $i+1/2, j$ are:

$$\psi_{i+1/2,j,d} = -\left(t_z - 1\right)\left(a_{csz} + b_{csz} + c_{csz}t_z\right) , \quad \text{(A.8)}$$

$$\psi_{M,i+1/2,j,d} = -\left(t_z - 1\right)\left(c_{csz} + t_z\left(3(a_{csz} + b_{csz}) - 2c_{csz}\left(1 - 2t_z\right)\right)\right) . \quad \text{(A.9)}$$

Cell i, j Integral Quantities

As shown in Fig. 3.2, the interior of cell i, j can be classified as 1 of 5 possible cases. The integration required by the definitions of Eqs. (3.9) is trivial for case 1 and case 5. Integration of the nonzero portions of $\widetilde{\psi}_{csz}(s,t)$ for cases 2-4 was carried out by decomposing the nonzero portion of cell i, j into N_T individual triangles $\mathbf{T_k}$ as shown in Fig. 3.3. With this notation, we can define the cell unknowns as being:

$$\psi_{A,i,j,d} = \sum_{k=1}^{N_T} \int\int_{\mathbf{T_k}} P_0(s,t)\hat{\psi}_{csz}(s,t)dsdt\,, \quad \text{(A.10)}$$

$$\psi_{X,i,j,d} = \sum_{k=1}^{N_T} 3\int\int_{\mathbf{T_k}} P_{1S}(s,t)\hat{\psi}_{csz}(s,t)dsdt\,, \quad \text{(A.11)}$$

$$\psi_{Y,i,j,d} = \sum_{k=1}^{N_T} 3\int\int_{\mathbf{T_k}} P_{1T}(s,t)\hat{\psi}_{csz}(s,t)dsdt\,. \quad \text{(A.12)}$$

We then integrate over each T_k by applying the definitions of Barycentric integration:

$$\int_{\mathbf{T_k}} f(\mathbf{r})dr = 2A_k \int_0^1 \int_0^{1-\lambda_2} f\left(\lambda_1\mathbf{v_1} + \lambda_2\mathbf{v_2} + \left(1 - \lambda_1 - \lambda_2\mathbf{v_3}\right)d\lambda_1 d\lambda_2\,, \quad \text{(A.13)}$$

where A_k is the area of $\mathbf{T_k}$ and we have transformed the $f(s,t)$ using the below transformation:

$$s = \lambda_1 s_1 + \lambda_2 s_2 + \left(1 - \lambda_1 - \lambda_2\right)s_3\,, \quad \text{(A.14)}$$

$$t = \lambda_1 t_1 + \lambda_2 t_2 + \left(1 - \lambda_1 - \lambda_2\right)t_3\,, \quad \text{(A.15)}$$

and we refer to the vertices of $\mathbf{T_k}$ as shown in Fig. A.1. For any individual triangle

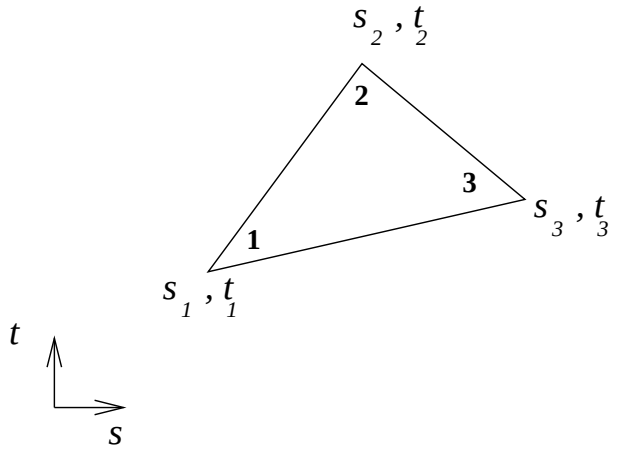

Fig. A.1. Coordinates of $\mathbf{T_k}$.

$\mathbf{T_k}$ we have the following:

$$\int\int_{\mathbf{T_k}} P_0(s,t)\hat{\psi}_{csz}(s,t)dsdt = A_k\left(a_{csz} - b_{csz} - c_{csz} + \frac{2b_{csz}}{3}(s_1+s_2+s_3) + \frac{2c_{csz}}{3}(t_1+t_2+t_3)\right), \quad \text{(A.16)}$$

$$3\int\int_{\mathbf{T_k}} P_{1S}(s,t)\hat{\psi}_{csz}(s,t)dsdt = A_k\,(3(b_{csz} - a_{csz} + c_{csz}) + (2a_{csz} - 4b_{csz} - 2c_{csz})(s_1+s_2+s_3) - 2c_{csz}(t_1+t_2+t_3) + 2b_{csz}(s_1^2+s_2^2+s_3^2) + 2b_{csz}(s_1s_2+s_1s_3+s_2s_3) + c_{csz}s_1(2t_1+t_2+t_3) + c_{csz}s_2(t_1+2t_2+t_3) + c_{csz}s_3(t_1+t_2+2t_3)), \quad \text{(A.17)}$$

$$3\int\int_{\mathbf{T_k}} P_{1T}(s,t)\hat{\psi}_{csz}dsdt = A_k\,(3(b_{csz} - a_{csz} + c_{csz}) + (2a_{csz} - 2b_{csz} - 4c_{csz})(t_1+t_2+t_3) - 2b_{csz}(s1+s2+s3) + 2c_{csz}(t_1^2+t_2^2+t_3^2) + b_{csz}s_1(2t_1+t_2+t_3) + b_{csz}s_2(t_1+2t_2+t_3) + b_{csz}s_3(t_1+t_2+2t_3) + 2c_{csz}(t_1t_2+t_1t_3+t_2t_3)), \quad \text{(A.18)}$$

where Eq. (A.16), Eq. (A.17), and Eq. (A.18) respectively compute the $\psi_{A,i,j,d}$, $\psi_{X,i,j,d}$, and $\psi_{Y,i,j,d}$ components of Eqs. (A.12) respectively.

VITA

Peter Gregory Maginot received dual B.S. degrees at Texas A&M University in the areas of nuclear engineering and radiological health engineering in May 2009. He enrolled as a graduate student seeking a M.S. degree in nuclear engineering in August 2009 and completed his M.S. degree in December 2010. Research areas of interest include particle transport methods development, coupled radiation hydrodynamics simulation, and associated areas of high performance computing.

Mr. Maginot may be contacted by mail through the Texas A&M University Nuclear Engineering Department, 3133 TAMU, College Station, TX, 77843. Electronically, he may be reached at: pmaginot@tamu.edu.